REVIEW   **Open Access**

Precise orbit determination for BDS satellites

Qile Zhao[1], Jing Guo[1*] , Chen Wang[1,2], Yifei Lyu[1], Xiaolong Xu[1], Chao Yang[1] and Junqiang Li[3]

Abstract

Since the first pair of BeiDou satellites was deployed in 2000, China has made continuous efforts to establish its own independent BeiDou Navigation Satellite System (BDS) to provide the regional radio determination satellite service as well as regional and global radio navigation satellite services, which rely on the high quality of orbit and clock products. This article summarizes the achievements in the precise orbit determination (POD) of BDS satellites in the past decade with the focus on observation and orbit dynamic models. First, the disclosed metadata of BDS satellites is presented and the contribution to BDS POD is addressed. The complete optical properties of the satellite bus as well as solar panels are derived based on the absorbed parameters as well the material properties. Secondly, the status and tracking capabilities of the L-band data from accessible ground networks are presented, while some low earth orbiter satellites with onboard BDS tracking capability are listed. The topological structure and measurement scheme of BDS Inter-Satellite-Link (ISL) data are described. After highlighting the progress on observation models as well as orbit perturbations for BDS, e.g., phase center corrections, satellite attitude, and solar radiation pressure, different POD strategies used for BDS are summarized. In addition, the urgent requirement for error modeling of the ISL data is emphasized based on the analysis of the observation noises, and the incompatible characteristics of orbit and clock derived with L-band and ISL data are illuminated and discussed. The further researches on the improvement of phase center calibration and orbit dynamic models, the refinement of ISL observation models, and the potential contribution of BDS to the estimation of geodetic parameters based on L-band or ISL data are identified. With this, it is promising that BDS can achieve better performance and provides vital contributions to the geodesy and navigation.

Keywords: BDS, Orbit and clock, Solar radiation pressure, Attitude, Phase center correction, Inter-satellite-link

Introduction

Global Navigation Satellite System (GNSS) is the essential technology to provide space and time information. China decided to establish its own independent GNSS in 1980 s, named as BeiDou Navigation Satellite System (BDS) (Yang et al., 2017a). Twenty years later, the BeiDou Navigation Satellite Demonstration System (BDS-1) with three GEostationary Orbit (GEO) satellites were successfully deployed to provide the regional Radio Determination Satellite Service (RDSS) in 2003. With the launch of the first Medium Earth Orbit (MEO) satellite in 2007, the

BeiDou Navigation Satellite (regional) system (BDS-2) was constructed to provide the regional radio navigation satellite service. This phase was completed when an official declaration of the regional navigation service around Asia-Pacific region was made at the end of 2012. At that time, the space segment consisted of 5 GEO, 4 MEO, and 5 Inclined GeoSynchronous Orbit (IGSO) satellites. Soon after, the BeiDou Navigation Satellite System with global coverage (BDS-3) began to build with two steps. In the first step 2 IGSO and 3 MEO satellites were deployed from March 2015 to February 2016 for the In-Orbit Validation (IOV) of the new features of the BDS-3 satellites, including signals, Inter-Satellite Link (ISL) technology, and onboard frequency standards (Zhao et al., 2018). In the second step a total of 27 satellites with Full-Orbit-Capability (FOC), including 3 GEO, 3 IGSO, and 24 MEO, were launched within the following four years. The

*Correspondence: jingguo@whu.edu.cn
[1] GNSS Research Center, Wuhan University, 129 Luoyu Road, Wuhan 430079, China
Full list of author information is available at the end of the article
This article belongs to the Topical Collection: BDS/GNSS high-precision products: strategies, services, and applications.

global Positioning, Navigation, and Timing (PNT) services have been officially provided since 31 July, 2020.

BDS together with other GNSS systems, e.g., Global Positioning System (GPS), Global Navigation Satellite System (GLONASS), and Galileo navigation satellite system (Galileo), can offer high-accuracy positioning to meet the needs of scientific and engineering applications. Furthermore, it helps reduce the spurious signals in the GPS-derived geodetic parameters, e.g., Earth Orientation Parameters (EOP) as well as geocenter position, and improve the realization of the Terrestrial Reference Frame (TRF), which is one of the core tasks of geodesy. All of these rely on the high quality orbit and clock products, which can be determined accurately with precise modeling of well-distributed measurements and orbit dynamic perturbations. The initial access to the BDS signals was provided by the BDS Experimental Tracking Stations (BETS) established by the GNSS Research Center of Wuhan University (WU) since March 2011 (Shi et al., 2012). Besides, the networks of International GNSS Monitoring and Assessment System (iGMAS) (Jiao et al., 2011) and International GNSS Service (IGS) Multi-GNSS EXperiment (MGEX) (Montenbruck et al., 2017a) project are also the essential data resources for the BDS analysis. For BDS-3 POD, the ISL measurements can also be used alone or in a combination with L-band data.

With these types of data, precise BDS orbits and clocks can be determined. The absence of accurate observation models, e.g., Phase Center Corrections (PCC) for the receiving and transmitting antenna, was noticed (Dilssner et al., 2014). The special yaw attitude control mode has been revealed for BDS-2 IGSO and MEO (Guo & Zhao, 2014; Dai et al., 2015) as well as for BDS-3 (Zhao et al., 2018; Dilssner 2017; Wang et al., 2018), and its impacts on the orbit determination were investigated for BDS-2 IGSO and MEO satellites (Wang et al., 2013; Guo et al., 2013). Moreover, the deficiencies of the widely used Extend CODE (Center for orbit determination in Europe) Orbit Model (ECOM) of Solar Radiation Pressure (SRP) (Beutler et al., 1994) for satellites in the Orbit-Normal (ON) mode and with elongated shape were observed (Arnold et al., 2015; Dilssner et al., 2018). Although dramatic improvement of orbit quality was obtained due to the improvement of POD strategy as well as observation and orbit dynamic models, the BDS orbit consistency is still about 2-times worse than that of GPS and Galileo (Sośnica et al., 2020).

The aim of this article is to develop the methodology to improve BDS orbit quality and make the further contribution to the estimation of geodetic parameters. It starts with the current deployment status of BDS constellation ("Status of BDS constellation" section), followed by the disclosed metadata from China Satellite

Navigation Office (CSNO) ("Metadata of BDS satellites" section). The evolution and status of the ground tracking networks and Low Earth Orbit (LEO) satellites with BDS tracking capability are presented in "Tracking data" section. The improvements and the remaining deficiencies of observation and orbit models are addressed separately in "Measurement models" and "Dynamic models" sections. The strategy for the orbit and clock determination with ground tracking data, LEO onboard data, and ISL data are presented in "Precise orbit and clock determination" section. The incompatible orbit and clock solutions derived from the ISL and L-band data are also discussed in "Precise orbit and clock determination" section, and the contribution of BDS to the estimation of geodetic parameters are presented in "Contributions to geodetic parameters estimation" section. Section "Summary and conclusion" summarizes the findings and the areas for further study.

Status of BDS constellation

For BDS-1 two primary operational GEO satellites, namely BeiDou-1A and BeiDou-1B, were launched on 31 October 2000 and 21 December 2000, respectively. A backup satellite BeiDou-1C was then launched on 24 May 2003. All satellites were manufactured by China Academy of Space Technology (CAST) based on the DongFang-Hong-3 (DFH-3) satellite bus with a 5-year design life. Currently, all of them are out of service.

BDS-2 was initiated with the launch of the first MEO satellite (M01) on 13 April 2007. Up to the preparation of this article, a total of 20 satellites, including 8 GEO satellites, 7 IGSO satellites, and 5 MEO satellites, have been deployed, among which 15 satellites are fully operational. For the rest, the BDS-2 M01 was discarded due to an apparent clock problem (Hauschild et al., 2011), and other 3 GEO satellites and 1 MEO satellite are inactive. All the satellites are manufactured by CAST based on the DFH-3A satellite bus and use the Rubidium Atomic Frequency Standards (RAFS) from China and Europe as the primary and backup clock, respectively.

For the in-orbit validation, BDS-3 experimental (BDS-3s) constellation consists of 1 IGSO satellite (I2S) and 2 MEO satellites (M1S and M2S) made by CAST as well as 1 IGSO satellite (I1S) and 1 MEO satellite (M3S) satellites manufactured by Shanghai Engineering Center for Microsatellites (SECM) of the China Academy of Science (CAS). It was initiated on 30 March 2015 with the deployment of the first IGSO satellite. With respect to BDS-2, different satellite buses, newly designed signals (B1C, B2a, and B2b), ISL in Ka band, updated RAFSs, and new Passive Hydrogen Masers (PHMs), are used. Due to the failure of navigation signal transmitter, no signals are available for M3S (Zhou et al., 2018). Currently, the rest

BDS-3s satellites are also decommissioned for transmitting signals.

Following the success of BDS-3s, the BDS-3 constellation with the full-orbit capability started to build with the launch of the first satellite pair on 5 December 2017. Currently, 3 GEO satellites, 3 IGSO satellites, and 14 MEO satellites manufactured by CAST are active, whereas 10 MEO satellites made by SECM are also in operation to provide global PNT services. The new technology successfully validated by BDS-3s satellites is also used in BDS-3 missions. Besides the primary Ka-band, the laser ISL is also implemented (Zheng, 2020). For SECM MEO satellites, two PHMs are used as the primary frequency standard, while two improved Chinese RAFS clocks are used as the backup. For CAST MEO satellites launched before 2019, four RAFS clocks are equipped, whereas two PHM clocks are used as the primary frequency standard for CAST GEO satellites and IGSO satellites. However, for the rest CAST MEO satellites, only one PHM clock is carried (Chen & Wu, 2020). Table 1 lists the in-orbit status of BDS constellation as 9 September 2021, and the readers can refer the website of Test and Assessment Research Center (TARC) of CSNO for the latest status of BDS system (http://www.csno-tarc.cn/system/constellation).

Metadata of BDS satellites

Satellite metadata, the definition and description of satellite properties, includes unique identifiers like Satellite Vehicle Number (SVN), time of life, the geometry properties (e.g., attitude, the position of mass center, transmit antenna and laser retroreflector array, the shape as well as the dimensions of satellite panels or bus), and the physical properties (e.g., materials, mass, transmit power of signals, optical and thermal properties). They are vital for the accurate modeling of GNSS satellites, particularly for the non-conservative perturbation modeling.

At the end of 2019, CSNO disclosed the metadata for BDS-2 and BDS-3 satellites (CSNO 2019a). The Phase Center Offsets (PCO) of transmitter antenna in B1, B2, and B3 frequency are archived in IGS Antenna Exchange Format (ATX) and will be discussed in "Phase center correction" subsection. While the rests are published in another file containing the satellite identifiers (SVN, Pseudorandom Noise/PRN, COSPARID), block type, active period, mass, laser retroreflector eccentricities, satellite effective surfaces, and the absorption coefficient of satellite bus as well as solar panels. Besides, the attitude law is described in the document 'Definitions and descriptions of BDS/GNSS satellite parameters for high precision application' (CSNO, 2019b) and will be described in "Yaw attitude" subsection. These disclosed metadata can be used for the precise analysis of BDS

data. However, it is not enough for orbit dynamic modeling, particularly the SRP, Earth Radiation Pressure (ERP) and antenna thrust, as the specular and diffuse reflection coefficients as well as the signal transmit power are missing.

For illustration purpose, Fig. 1 shows the artist's impression of BDS-3 GEO, IGSO, CAST MEO and SECM MEO satellites from TARC of CSNO and SECM. Those can be found in Yang et al. (2017a) for BDS-2 GEO, IGSO and MEO satellites. Table 2 lists their dimensions, mass, area of solar panels, as well as the ratio of Z to X panel area. Here, the directions of satellite body reference frame follow the IGS conventions (Montenbruck et al., 2015b). As mentioned earlier, BDS-1 satellites are manufactured based on the DFH-3 satellite bus with a size of 2.2 m × 1.72 m × 2.0 m, while the DFH-3A satellite bus is used for all BDS-2 satellites with the similar dimension as its predecessor. Additionally, BDS-2 GEO satellite carries a large Communication Antenna (CA) folded on the $+X$ surface connecting to the $+Z$ surface for time synchronization and RDSS telecommunications with an area approximately 3.14 m² (Wang et al., 2019a). BDS-3 satellites are produced by different manufactures based on their own satellite buses. All GEO and IGSO satellites are manufactured by CAST based on the DFH-3B platform (Chen & Wu, 2020). Moreover, one can see from Fig. 1 that BDS-3 GEO and IGSO are equipped with two and one hexagonal antennas folded on the $\pm X$ and $+X$ surfaces, respectively, while there are two smaller circle antennas on IGSO satellite for the in-orbit validation of high-speed data transformation as well as procession (Chen & Wu, 2020). For CAST MEO satellites, a dedicated T-shaped platform is developed to facilitate the lunch of multiple satellites at same time (Zhang et al., 2020), and there could be an additional panel on the $-X$ surface flipped up for Search and Rescue (SAR) service. However, the satellite body of BDS-3 CAST MEO satellites published by CSNO is a standard cuboid, but it is a bit far from the real. The more precise dimensions are reported by Duan et al. (2021b) and listed in Table 2.

As a new provider of BDS satellites, SECM produces their own satellite platform. Most of SECM satellites are manufactured based on the same bus (SECM-A) expect for M11 and M12 (SECM-B), which have slightly different shapes, as shown in the CSNO released metadata.
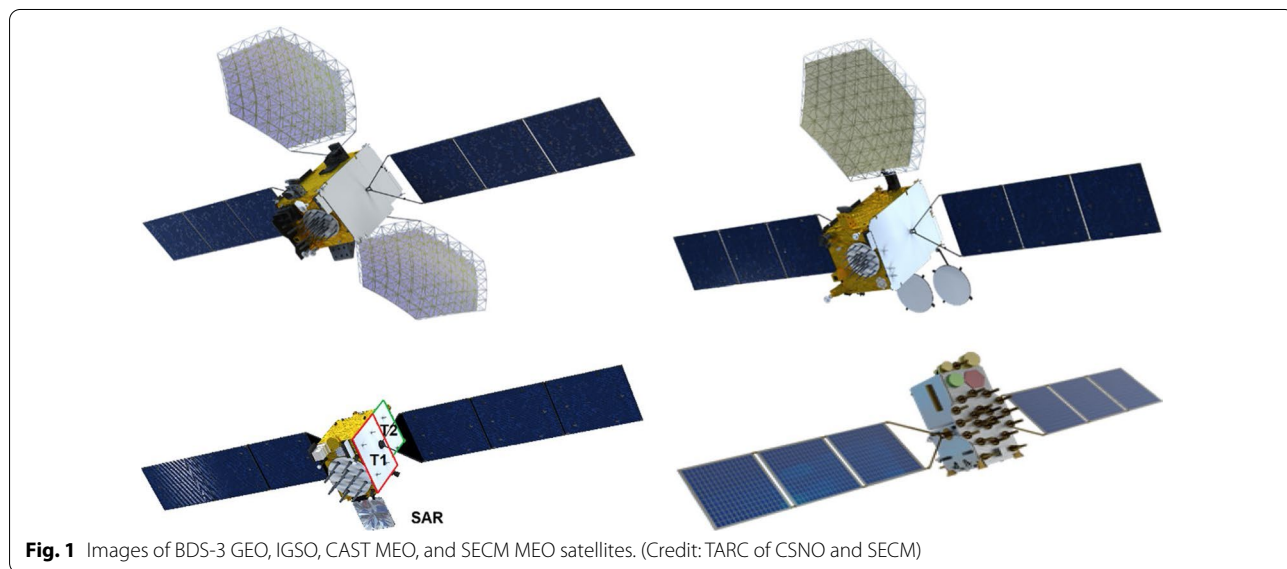
The ratio of Z to X panel areas listed in Table 2 indicates stretched degree of the satellite bus. The closer to 1 this value is, the closer to a cubic the satellite bus will be. Hence, BDS-3 GEO, IGSO, and MEO satellites are much more elongated than their counterparts of BDS-2 satellites. However, the mass of BDS-3 GEO and IGSO is about 1.5 times the weight of BDS-2 satellites,

Zhao *et al. Satellite Navigation*   (2022) 3:2

Page 4 of 24

Table 1 The status and information of BDS satellites as 9 September 2021

PRN	IGS-SVN	NORADID	SVN	Position	Satellite type	Clock type	Manufacture	Launch date
C01	C020	44,231	GEO-8	140.0°E	BDS-2	RAFS	CAST	2019-05-17
C02	C016	38,953	GEO-6	80.3°E	BDS-2	RAFS	CAST	2012-10-25
C03	C018	41,586	GEO-7	144.5°E	BDS-2	RAFS	CAST	2016-06-12
C04	C006	37,210	GEO-4	160.0°E	BDS-2	RAFS	CAST	2010-11-01
C05	C011	38,091	GEO-5	58.75°E	BDS-2	RAFS	CAST	2012-02-25
C06	C005	36,828	IGSO-1	~117°E	BDS-2	RAFS	CAST	2010-08-01
C07	C007	37,256	IGSO-2	~119°E	BDS-2	RAFS	CAST	2010-12-18
C08	C008	37,384	IGSO-3	~117°E	BDS-2	RAFS	CAST	2011-04-10
C09	C009	37,763	IGSO-4	~95°E	BDS-2	RAFS	CAST	2011-07-27
C10	C010	37,948	IGSO-5	~96°E	BDS-2	RAFS	CAST	2011-12-02
C11	C012	38,250	MEO-3	Within A6 and A7	BDS-2	RAFS	CAST	2012-04-30
C12	C013	38,251	MEO-4	Within A7 and A8	BDS-2	RAFS	CAST	2012-04-30
C13	C017	41,434	IGSO-6	~94°E	BDS-2	RAFS	CAST	2016-03-30
C14	C015	38,775	MEO-6	Within B3 and B4	BDS-2	RAFS	CAST	2012-09-19
C16	C019	43,539	IGSO-7	~112°E	BDS-2	RAFS	CAST	2018-07-10
C19	C201	43,001	MEO-1	B7	BDS-3	RAFS	CAST	2017-11-05
C20	C202	43,002	MEO-2	B8	BDS-3	RAFS	CAST	2017-11-05
C21	C206	43,208	MEO-3	B5	BDS-3	RAFS	CAST	2018-02-12
C22	C205	43,207	MEO-4	B6	BDS-3	RAFS	CAST	2018-02-12
C23	C209	43,581	MEO-5	C7	BDS-3	RAFS	CAST	2018-07-29
C24	C210	43,582	MEO-6	C1	BDS-3	RAFS	CAST	2018-07-29
C25	C212	43,603	MEO-11	C2	BDS-3	PHM	SECM	2018-08-25
C26	C211	43,602	MEO-12	C8	BDS-3	PHM	SECM	2018-08-25
C27	C203	43,107	MEO-7	A4	BDS-3	PHM	SECM	2018-01-12
C28	C204	43,108	MEO-8	A5	BDS-3	PHM	SECM	2018-01-12
C29	C207	43,245	MEO-9	A2	BDS-3	PHM	SECM	2018-03-30
C30	C208	43,246	MEO-10	A3	BDS-3	PHM	SECM	2018-03-30
C31	C101	40,549	IGSO-1 S	/	BDS-3s	PHM	SECM	2015-03-30
C32	C213	43,622	MEO-13	B1	BDS-3	RAFS	CAST	2018-09-19
C33	C214	43,623	MEO-14	B3	BDS-3	RAFS	CAST	2018-09-19
C34	C216	43,648	MEO-15	A7	BDS-3	PHM	SECM	2018-10-15
C35	C215	43,647	MEO-16	A1	BDS-3	PHM	SECM	2018-10-15
C36	C218	43,706	MEO-17	C4	BDS-3	RAFS	CAST	2018-11-19
C37	C219	43,707	MEO-18	C6	BDS-3	RAFS	CAST	2018-11-19
C38	C220	44,204	IGSO-1	~ 113.2°E	BDS-3	PHM	CAST	2019-04-20
C39	C221	44,337	IGSO-2	~ 106.6°E	BDS-3	PHM	CAST	2019-06-25
C40	C224	44,709	IGSO-3	~ 104.3°E	BDS-3	PHM	CAST	2019-11-05
C41	C227	44,864	MEO-19	B2	BDS-3	PHM	CAST	2019-12-16
C42	C228	44,865	MEO-20	B4	BDS-3	PHM	CAST	2019-12-16
C43	C226	44,794	MEO-21	A6	BDS-3	PHM	SECM	2019-11-23
C44	C225	44,793	MEO-22	A8	BDS-3	PHM	SECM	2019-11-23
C45	C223	44,543	MEO-23	C3	BDS-3	RAFS	CAST	2019-09-23
C46	C222	44,542	MEO-24	C5	BDS-3	RAFS	CAST	2019-09-23
C56	C104	40,938	IGSO-2 S	/	BDS-3s	PHM	CAST	2015-09-30
C57	C102	40,749	MEO-1 S	/	BDS-3s	RAFS	CAST	2015-07-25
C58	C103	40,748	MEO-2 S	/	BDS-3s	RAFS	CAST	2015-07-25
C59	C217	43,683	GEO-1	~ 140°E	BDS-3	PHM	CAST	2018-11-01
C60	C229	45,344	GEO-2	~ 80°E	BDS-3	PHM	CAST	2020-03-09
C61	C230	45,807	GEO-3	~ 110.5°E	BDS-3	PHM	CAST	2020-06-23

SVN satellite vehicle number

PRN pseudorandom noise

Fig. 1 Images of BDS-3 GEO, IGSO, CAST MEO, and SECM MEO satellites. (Credit: TARC of CSNO and SECM)

Table 2 Geometry dimensions of BDS satellite bus and mass

Constellation	Satellite type	Bus	Mass (kg)	X (m)	Y (m)	Z (m)	Area of solar panels (m^2)	Ratio of Z/X area
BDS-1	GEO	DFH-3	~ 2200	2.20	1.72	2.00	/	0.91
BDS-2	GEO	DFH-3A	~ 2000	2.00	1.72	2.20	22.7	1.10
	IGSO	DFH-3A	~ 1280	2.00	1.72	2.20	22.7	1.10
	MEO	DFH-3A	~ 1185	2.00	1.72	2.20	22.7	1.10
BDS-3	GEO	DFH-3B	~ 2970	2.10	2.36	3.60	35.4	1.71
	IGSO	DFH-3B	~ 2910	2.10	2.36	3.60	35.4	1.71
	MEO	T-shaped (T1)	~ 1000	1.68	1.30	1.30	20.44	~1.31
		T-shaped (T2)		1.00	1.30	0.85		
		T-shaped (SAR)		0.85	1.30	0.00		
		SECM-A	~ 1050	2.55	1.02	1.51	10.8	0.59
		SECM-B	~ 1050	2.80	0.92	1.35	10.8	0.48

whereas BDS-3 MEO satellites are lighter than that of BDS-2. Hence, the deficiencies of non-gravitational perturbations will be more noticeable for BDS-3 due to the large area-to-mass ratio compared to BDS-2. Moreover, BDS-3 SECM MEO satellites are stretched along different direction as BDS-3 CAST MEO satellites, hence, the characteristics of orbit errors will be different and will be presented and discussed in "Solar radiation pressure (SRP)" subsection.

Lack of the reflection and diffusion properties limits the accurate modeling of SRP and ERP. For BDS-2 satellites, the optical properties including materials are reported by Chen et al. (2019) from CAST. In general, the satellite surfaces are covered by three kinds of materials, i.e., Multi-Layer Insulation (MLI) blankets with an absorbed coefficient (α) of 0.36 and a specularly reflected coefficient (ρ) of 0.0, Optical Solar Reflectors (OSRs) with $\alpha = 0.135$ and $\rho = 0.865$, and anti-static white paint with $\alpha = 0.23$ and $\rho = 0.0$. The $+X$, $-X$, and $-Z$ surfaces are covered by MLI entirely. The area of OSRs on $+Y$ and $-Y$ surfaces is about 2.223 and 2.18 m^2, respectively, while the rest are MLIs. The $+Z$ surface consists of anti-static white paint (about 1.039 m^2) and MLIs. Table 3 lists the corresponding optical properties for all surfaces, which are slightly different from the CSNO released values for the $+Y$, $-Y$, and $+Z$ surfaces with two kinds of materials. Solar panels use the silicon photovoltaic solar cells, and the absorbed, reflected, and diffused properties are 0.72, 0.238, and 0.042, respectively (Chen et al., 2019). While the optical values for the CA antenna of BDS-2 GEO are assumed the same as that of $-Z$ to facilitate the SRP modeling.

Table 3 The optical properties for BDS-2 and BDS-3 satellites

Satellites	Panel	Absorbed (α)	Reflected (ρ)	Diffused (δ)
BDS-2 GEO/IGSO/MEO	+X	0.360	0.000	0.640
	−X	0.360	0.000	0.640
	+Y	0.246	0.437	0.317
	−Y	0.249	0.428	0.323
	+Z	0.321	0.000	0.679
	−Z	0.360	0.000	0.640
	Solar panels	0.720	0.238	0.042
BDS-2 GEO	CA	0.360	0.000	0.640
BDS-3 GEO/IGSO	+X	0.350	0.000	0.650
	−X	0.350	0.000	0.650
	+Y	0.135	0.865	0.000
	−Y	0.135	0.865	0.000
	+Z	0.870	0.130	0.000
	−Z	0.870	0.130	0.000
	Solar panels	0.920	0.080	0.000
BDS-3 MEO CAST	+X	0.350	0.00	0.650
	−X	0.615	0.385	0.000
	+Y	0.135	0.856	0.000
	−Y	0.135	0.856	0.000
	+Z	0.920	0.080	0.000
	−Z	0.350	0.00	0.650
	Solar panels	0.920	0.080	0.000
BDS-3 MEO SECM	+X	0.200	0.800	0.000
	−X	0.200	0.800	0.000
	+Y	0.200	0.800	0.000
	−Y	0.200	0.800	0.000
	+Z	0.200	0.800	0.000
	−Z	0.200	0.800	0.000
	Solar panels	0.920	0.080	0.000

For BDS-3, the optical properties can be roughly derived by taking BDS-2 satellites as the reference. All BDS-3 satellites use triple junction GaAs (gallium arsenide) solar cells for solar panels, and their absorption property is 0.92 and no diffusion. The satellites are also wrapped up with MLIs, as shown in Fig. 1. It seems that $+X$ and $-X$ surfaces of GEO and IGSO satellites are covered by this material completely, while the $+Y$ and $-Y$ surfaces are made of OSRs. For $+Z$ and $-Z$ surfaces, the CSNO disclosed absorbed property is 0.87, which is larger than that of all materials used by BDS-2 satellites. As no further information is available, we simply assume the specularly reflected coefficient of 0.13. More details on the additional antenna mounted on IGSO and GEO satellites are also missing, hence, their optical properties and dimensions are not presented in Table 3. For CAST MEO satellites, $+X$ and $-Z$ surfaces are covered by MLIs totally, while the $+Y$ and $-Y$ surfaces are made of OSRs. The $-X$ surface

in fact consists of two parts: one with an area of 1.11 m^2 is OSR, and the other with an area of 1.76 m^2 has high absorbed property of 0.92. The triple junction GaAs used by solar panels also has the same absorbed coefficient. In addition, $+Z$ surface also has the same absorbed property. For these surfaces, no diffusion is assumed. Table 3 lists the average optical properties. Hence, the absorbed coefficient is different from CSNO released values for $-X$ surface. Besides, the details on the SAR antenna are also missing. For SECM satellites, it is reported that all the six surfaces have the same absorption coefficient of 0.20 by CSNO. We assume the OSRs is used, hence, a specular reflection coefficient is 0.80.

It is worth to mention that the optical properties listed in Table 3 are quite coarse, particularly for BDS-3 SECM MEO satellites. However, with the real tracking data, they can be calibrated as shown by Duan et al. (2019, 2021b).

Zhao *et al. Satellite Navigation*   (2022) 3:2

Page 7 of 24

Tracking data

### L-band tracking data

Ground tracking stations

For ground tracking of BDS satellites, there are BETS and two accessible networks, i.e., iGMAS and IGS. The Cooperative Network for GIOVE Observations (CONGO) built by various German institutes (Montenbruck et al., 2011) and Australian Regional GNSS Network (ARGN) of Geoscience Australia also provide BDS observations. As the both contribute to IGS network, we do not discuss them here.

The BETS has been operated since March 2011 by GNSS Research Center of WU to monitor the PNT performance of BDS-2 system. This network comprises 15 stations, among which 6 stations are located outside China (Shi et al., 2012). All the stations are equipped initially with UB240-CORS receiver and UA240 high gain antenna manufactured by Beijing Unicore Communications Incorporation, and can track the GPS L1 and L2 as well as BDS B1I and B2I signals. Later some receivers were replaced by Trimble NetR9 to support Multi-GNSS research (Zhao et al., 2013). Currently, this network is decommissioned. However, it provided the initial tests of BDS-2 signals, and made BDS-2 constellation recognized in the GNSS community, particularly in the early age. The data can be provided by GNSS Research Center on request.

The iGMAS network is built by the iGMAS project aiming at monitoring and assessing the performance of Multi-GNSS system (Jiao et al., 2011). It consists of 31 globally distributed stations equipped with six types of receivers from three manufactures. All receivers can track BDS-2 B1I, B2I, and B3I signals. Currently all of them are also able to track the B1I, B3I, B1C, and B2a open service signals of BDS-3 satellites. Furthermore, B2b signal can be tracked by two kinds of receivers. These data can be downloaded by authorized parties from three data archive centers.

IGS initiated the MGEX project in the middle of 2011, and simultaneously built a network with Multi-GNSS tracking capability as its backbone. The IGS MGEX stations utilize diverse types of receivers mainly from Javad, Leica, NovAtel, Septentrio, and Trimble. In 2016, all MGEX stations were fully incorporated into the official IGS network (Montenbruck et al., 2017a). As September 2021, there are more than 250 Multi-GNSS stations tracking BDS signals, as shown in Fig. 2. The observations from the IGS Multi-GNSS network are freely available to users from IGS data centers.

Figure 3 shows the number of the iGMAS and MGEX stations which track BDS-2 and BDS-3 satellites since 2014. In general, the tracking capability of iGMAS stations is promoted gradually. For MGEX, the tracking
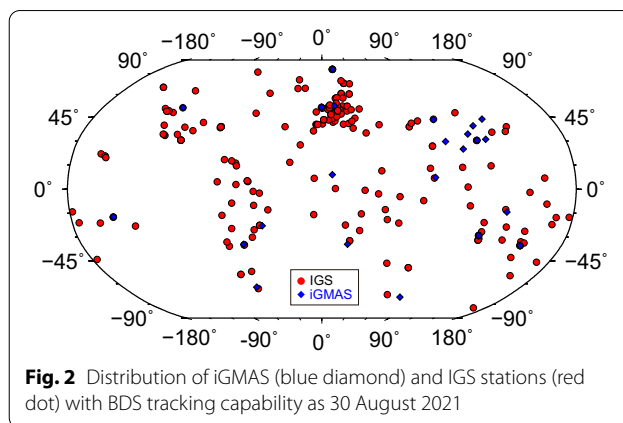

Fig. 2 Distribution of iGMAS (blue diamond) and IGS stations (red dot) with BDS tracking capability as 30 August 2021
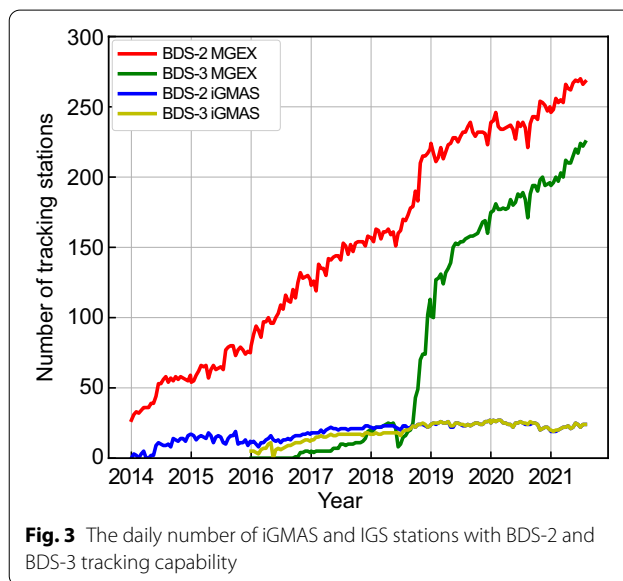
Fig. 3 The daily number of iGMAS and IGS stations with BDS-2 and BDS-3 tracking capability

capability for BDS-2 is also improved gradually, while a rapid change around the middle of 2018 is observed for BDS-3 due to the deployment of Trimble Alloy and the update of Trimble NetR9, Septentrio POLARX5/POLARX5TR.

However, not all deployed BDS-3 satellites can be tracked by each receiver, possibly due to the limitation of tracking channels or firmware. Figure 4 shows the daily number of IGS and iGMAS stations tracking the representative satellites, i.e., C19, C23, C32, C35, C38, C41, C56 and C59 from 2019 to 2021. The number of stations with C19 tracked represents those for tracking C19-C22 satellites, whereas that for C23 indicates those for satellites C23–C31, and the similar for the rest. In general, the early launched satellites can be tracked by more receivers. At the beginning of 2019, except for Javad TRE-3 Delta receiver and iGMAS receivers capable to track all deployed BDS-3 satellites, Trimble receivers can only

Fig. 4 The daily number of IGS and iGMAS stations tracking the representative BDS-3 satellites C19, C23, C32, C35, C38, and C59 since 2019
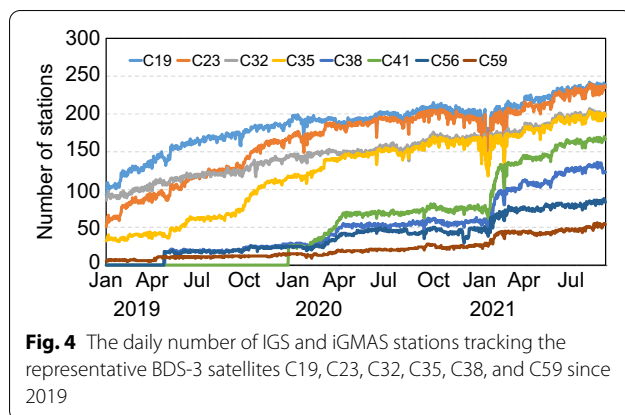
track the C19–C30 satellites, and Septentrio receivers with the latest firmware can only track C19–C22 and C32–C34 satellites. Hence, the number of the stations with C19 tracked is the greatest, then followed by C32. With the update of Trimble NetR9 as well as deployment of Trimble Alloy, the number of the stations tracking C23 increase gradually, and even exceeds that for C32. Thanks to the update of Septentrio firmware, C35 is tracked by more stations, and the number is over 100 by the end of 2019. Moreover, insignificant difference in the number of tracking stations can be observed for IGSO (C38–C40) and MEO satellites with PRN beyond 40 in 2019, as only iGMAS stations can track them. However, the situation changed at the beginning of 2020. Significant improvement can be observed during January 2021 due to the firmware updates of Septentrio receivers. The different tracking capability will impact the derived orbit quality.

LEO satellites

Besides ground tracking stations, there are a few LEO satellites equipped with GNSS receivers with BDS tracking capability, e.g., LING QIAO (Chen et al., 2016), FengYun-3C/3D (Li et al., 2020c), Luojia-1A (Wang et al., 2020d), and Tianping-1B (Zhao et al., 2020).

The LING QIAO satellite was launched on 4 September 2014, which is the China's first LEO mobile communication experimental satellite and carries two single-frequency GPS receivers for navigation and time synchronization. Besides, one independent single-frequency BDS receiver is also equipped for the in-orbit validation of its performance. However, the actual number of tracked BDS satellites is lower than the expected due to lower acquisition efficiency. Lack of dual-frequency observations limits the enhanced BDS POD with its onboard data.

The above problem is overcome by FengYun-3C satellite, which was launched on 23 September 2013,

and developed by the Meteorological Administration/ National Satellite Meteorological Center (CMA/NSMC) of China. This satellite carries a GNSS Occultation Sounder (GNOS) developed by the Center for Space Science and Applied Research (CSSAR) of CAS for positioning, and GPS L1/L2 and BDS B1I/B2I signals from up to six BDS satellites and more than eight GPS satellites can be tracked simultaneously. Zhao et al. (2017) reported that the accuracy is about 0.69, 0.62, 0.38 and 0.820 m for BDS B1I, B2I, GPS C/A, and P2 code measurements, respectively, and is around 2 mm for phase observations. However, the quality of observation drops gradually from 2013 to 2017 due to the aging of the GNOS receiver (Li et al., 2020d). With this data, the elevation-dependent group delay variations of BDS-2 satellites were analyzed, and the BDS orbits, particularly for GEO, are improved due to the rapid variation of the observation geometry (Zhao et al., 2017). As the successor of FengYun-3C, FengYun-3D carries an enhanced GNOS instrument with up to 17 and 12 tracking channels for GPS and BDS, respectively, resulting in much more observations than that of FengYun-3C. The same dual-frequency signals are tracked, and the loss of tracking GPS L2 and BDS B2I signals, especially at low elevations, has been improved. Hence, FengYun-3D is more stable and has continuous tracking capability than that of FengYun-3C. Thanks to the good performance, its onboard data combined with the FengYun-3C data are also used to enhance BDS POD (Li et al., 2020c).

Luojia-1A is a nanosatellite launched in June 2018 for the technology demonstration of LEO-based navigation signal augmentation as well as nigh-light remote sensing. This satellite is operated by WU and carries an onboard receiver with GPS/BDS dual-frequency tracking capability. However, due to the distribution and the number of BDS-2 satellites, the percentage of the epochs with more than four satellites tracked are around 57%. However, Wang et al. (2020b) shows that the accuracy of code and phase measurements is a few decimeters and millimeters, respectively. Hence, it has potential for BDS enhanced POD.

Tianping-1B is also a nanosatellite equipped with a Multi-GNSS receiver manufactured by Beijing Hexie Avionics Technology Co., Ltd. with 12 tracking channels for GPS and BDS separately (Zhao et al., 2020). Different from the receivers in the above LEO satellites, its receiver supports BDS-3 tracking and collects code and phase measurements on B1I and B3I frequencies. However, the signals from the BDS-3 satellites with PRN beyond 32 cannot be tracked. In average 8 and 10 satellites can be tracked for BDS and GPS, respectively. The accuracy of a few decimeters is achieved for code measurements. It is vital to analyze BDS-3 observations, but unfortunately

the data cannot be freely accessed. In "With ground and onboard L-band data" subsection, the contribution of LEO onboard data to BDS POD will be presented and discussed.

Inter-satellite link data

As one of the significant developments of BDS-3, ISL technology is employed for satellite communication as well as ranging to achieve global SAR service, POD, and time synchronization without the limitation of regional distribution of monitoring stations. Different from GPS BLOCK IIR satellites using Ultra-High Frequency band, the Ka band and laser ISL are used by BDS-3.

The Concurrent Spatial Time Division (CSTD) system is employed by BDS-3 ISL to ensure the safe and complete connection among the satellites (Yang et al., 2017b). The word 'concurrent' means that many links are formed simultaneously between the satellites within the constellation, however, there is only one for each satellite. Time-division technology allows each satellite to be connected to other satellites in deferent timeslots (3 s), while the satellite within the view of nadir region ($-$ 60°, 60°) can be targeted using a phased-array antenna, which can switch the beam direction by changing the feed phase of different array elements to implement spatial division. Moreover, the quick orientation of the phased-array antenna ensures the implement of dual one-way observation within 3 s. For ISL ranging, in each timeslot a pair of satellites send signals to each other in turn based on a predefined timeslot schedule, which arranges the order of connection among satellites and is updated weekly by the ground control segment. Within 3 s, the forward and backward links are established in each 1.5 s. Hence, a satellite can establish the links with up to 20 satellites or anchor stations within 60 s, and the links with the whole constellation can be completed in a relative short period to support POD and autonomous navigation (Zheng, 2020).

Figure 5 demonstrates the connection for C32 (M13, Slot-B1) with other BDS-3 MEO satellites. The red solid lines represent the continuous satellite links, while the blue dash lines are the discontinuous links. All MEO satellites are evenly distributed on three orbital planes. The satellite cannot connect with its adjacent satellite and the farthest satellite in the same plane due to the nadir angle above 60° as well as earth occlusion, while continuous links with the second and third nearest satellites in the same orbit plane can be formed. For the cross-orbit-plane links, there are four continuous and 12 discontinuous links. In addition, each IGSO and GEO satellite can establish discontinuous link with MEO satellites, while the IGSO satellites can be connected with each other.
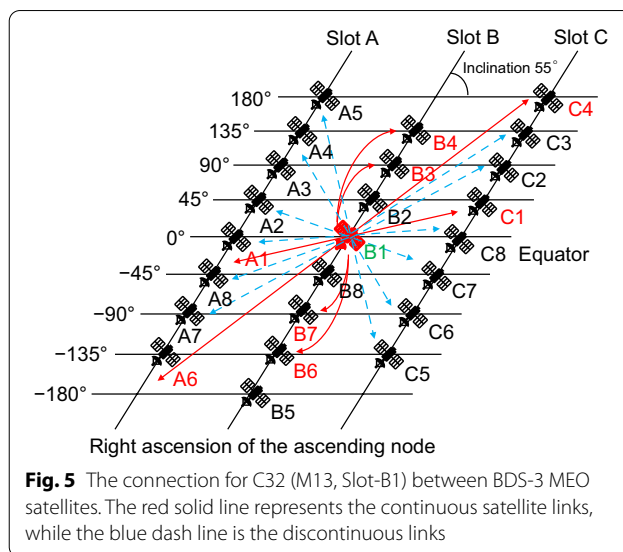
Fig. 5 The connection for C32 (M13, Slot-B1) between BDS-3 MEO satellites. The red solid line represents the continuous satellite links, while the blue dash line is the discontinuous links

Measurement models
Yaw attitude

The attitude of a GNSS satellite determines its orientation in space. It is essential for POD, as it has impact on the correction of observation errors and the modeling of non-gravitational perturbations. To ensure that users on Earth can effectively receive satellite signals, the transmitting antenna needs to point to the center of the Earth. Besides, the solar panels should be perpendicular to the direction of the Sun to ensure that the satellite has enough power supply. Under these two constrains, the nominal GNSS satellite attitude is determined. Usually, the *Z*-axis points to the Earth center, the *Y*-axis is the rotation axis of the solar panels and perpendicular to the direction of satellite to the Sun, and the *X*-axis completes the right-hand coordinate system and points to or away the velocity direction (Bar-Sever, 1996; Montenbruck et al., 2015b). However, the satellite does not always follow the nominal attitude law. The yaw maneuvers occur near the midnight and noon points of the orbital plane in low *β*-angle (the elevation angle of the Sun above the orbital plane) regime, as the required yaw rate exceeds the maximum value provided by the momentum wheel of satellite attitude control subsystem. This is termed as the midnight-/noon-turn maneuvers. Moreover, the eclipse maneuver happens when satellites cross the eclipse seasons, but only for GPS BLOCK IIA, due to the zero output of Sun sensors in the shadow of the Earth (Bar-Sever, 1996).

Usually, the attitude of different satellite blocks behaviors differently in the maneuver periods. The GEO satellites of BDS constellation adopts ON mode. In this case, the *Z*-axis points to the radial direction and the *X*-axis

points toward the along-track direction, which thus yields a zero-yaw angle. The Y-axis is perpendicular to the orbital plane and completes the right-hand frame. For BDS-2 IGSO and MEO satellites, the Yaw-Steering (YS) and ON modes are adopted. The transformation from YS to ON occurs when the absolute value of β angle is less than 4° and the absolute value of yaw angle (ψ angle) is no greater than 5° (Li et al., 2018), while the conditions for switching from ON to YS are $|\beta| > 4°$ and $|\psi| < 5°$. They present the yaw angles during the attitude switch period from the telemetry data for C08, C11 and C12 satellites, and the sudden rump-up and rump-down jumps instead of smooth switch can be clearly observed at the attitude switch points. With the Revise Kinematic Precise Point Positioning (RKPPP) approach proposed by Dilssner et al. (2011), the yaw angles were estimated with ground L-band measurements (Guo & Zhao, 2014; Dai et al., 2015). Almost the same conditions as Li et al. (2018) are derived by Dai et al. (2015). However, by assuming that the attitude mode will switch when the yaw angle is closest to the required orientation, Guo et al. (2017) derived the conditions for yaw attitude switch when $\mu = 90°$ and $|\beta|$ closest to 4°, where μ is the orbital angle. The above models are quite consistent because the yaw angles at orbit angle of 90° are about $\pm 4°$ for the low β angle. However, the analysis of all historical attitude switch events of BDS-2 IGSO and MEO satellites from 2016 to 2019 demonstrates that there are a few events occurring with $|\beta| > 4°$ for YS to ON and $|\beta| < 4°$ for ON to YS switch, respectively (Xia et al., 2019).

As the deficiency of widely used ECOM model for SRP modeling in the ON regime, the orbit accuracy degenerates significantly in this period. Hence, the newly launched BDS-2 as well as all BDS-3 IGSO and MEO satellites abandon the ON mode in low β regime, and the continuous YS model is used. In the estimation of the yaw angles, the behavior was first identified for BDS-2 I06, and the corresponding attitude model was proposed (Dilssner 2017; Wang et al., 2018). It is also confirmed that BDS-2 C14 (M06) has abandoned ON mode since September 2017. Generally, the model can predict the yaw behaviors quite well, however, a reverse midnight-turn maneuvers was first observed for I06 on DOY 171, 2017, when the β angle was less than 0.1° (Wang et al., 2018). Later more evens were identified for BDS-2 C13 and C14 when β angles falls into the range (0°, 0.14°) (Xia et al., 2019). Hence, a yaw bias of 0.14° is introduced to predict the features of the reverse midnight-turn yaw maneuvers (Xia et al., 2019).

The BDS-3 CAST MEO satellites obey the continuous yaw-steering law, while the yaw attitude for SECM MEO satellites was presented by Lin et al. (2018) and is confirmed by CSNO disclosed metadata (CSNO et al.

2019b). Generally, the yaw attitude with $\beta = \pm 3°$ is applied for the satellite when $|\beta|$ is less than 3°. When the Sun crosses the orbital plane, the sign of the yaw attitude will change in consistency with that of β angle. However, these behaviors could not be validated with L-band data due to near zero values of horizontal PCOs of the satellites. For BDS-3 IGSO satellites manufactured by CAST, the model proposed by Wang et al. (2018) can be used, but still needs further validation. High-rate Satellite Laser Ranging (SLR) and ISL measurements provide the possibility of assessment. With ISL data, the yaw attitudes of BDS-3 IGSO and MEO satellites are derived and analyzed by Yang et al. (2021), and the results clearly confirm the yaw attitude of BDS-3 CAST IGSO follows the model proposed by Wang et al. (2018), however, the yaw behaviors of SECM MEO satellites are occasionally different with the prediction of CSNO disclosed model.

Phase center correction

GNSS observations measure the geometric distance between the antenna phase center of a navigation satellite at signal emission time and the receiving antenna at signal reception time. The phase center is usually different from the Antenna mechanical Reference Points (ARP). Hence, high-precision GNSS applications require a set of PCCs to tie the GNSS measurements consistently to the ARP of the satellite and receiver antenna. Normally, the set of PCCs for the antenna phase center consists of PCO and Phase Center Variation (PCV).

For receiver antenna, the lack of consistent Multi-frequency Multi-GNSS PCCs limits the accurate modeling of GNSS data, particularly for the new systems. The official IGS ATX file contains dual-frequency PCCs of the GPS and GLONASS receiver antennas only. Hence, the values of GPS L1 and L2 were used for BDS data analysis. To overcome the dilemma, the independent PCO/PCV calibrations for BDS and Multi-GNSS signals were conducted and reported (Su et al., 2018; Wang et al., 2020a; Kröger et al., 2021; Krzan et al., 2020; Willi et al., 2020). The PCCs for GPS and BDS signals using the robotic method were calibrated (Su et al. 2018). The similar work was also carried out at CAS (Wang et al., 2020a). However, only two antennas, i.e., TRM5791.00 NONE and TRM59800.00 NONE, were calibrated. Since April 2019, the IGS ACs have carried out the third run of reprocessing the full history of GNSS data in a fully consistent way using the latest models and methodology. The Multi-frequency Multi-GNSS calibration results for a set of antennas were provided by Geo++ for incorporating Galileo into analysis (Wübbena et al., 2019), while the PCCs for BDS open-service signals are also provided for some types of antennas, and they can be used for PCC calibration of the transmitter antenna.

For the satellite antenna, conventional PCOs were initially adopted and recommended by IGS MGEX for BDS-2 based on the approximate spacecraft body dimensions. Afterwards, the PCCs of satellite antennas were calibrated in the IGS08 frame (Dilssner et al., 2014; Guo et al., 2016a; Huang et al., 2018). However, their estimates show significant differences in the Z-offset, especially for IGSO satellites (at meter level), possibly caused by data processing methods and software. Furthermore, the FengYun-3C onboard data were used to extend the PCV estimation of BDS-2 IGSO and MEO (Qu 2021). For the BDS-3 satellites, although the ground calibrated PCO values have already been provided by the CSNO, the preliminary estimates of satellite antenna PCCs in the ITRF14 frame are carried out by Yan et al. (2019a, b), Springer et al. (2020), and Xia et al. (2020). The results show that the discrepancy between the estimated and the ground calibrated PCOs is within a decimeter, and the estimation is affected by the receiver antenna models as well as the SRP model. For the first two estimates, the antenna corrections for BDS B1I and B3I signals are replaced by that of GPS L1 and L2. For the last one, although the receiver antenna PCCs are modeled, only PCOs are calibrated within ITRF14 frame without regards of PCCs. Qu et al. (2021) estimated PCOs and PCVs for BDS-3 IGSO and MEO satellites in ITRF14 and IGS Repro3 frame. Villiger et al. (2021) also calibrated the PCCs for BDS in the IGS Repro3 frame. The two estimates show a quite good consistency and confirm that BDS-3 MEO satellites have an offset of about 10 cm for Z-PCO in IGS Repro3 frame with respect to the CSNC disclosed values. Excellent consistency results are also obtained for the estimates in ITRF14 frame. The PCCs calibration of BDS transmitter antennas facilitates the consistency analysis of Multi-GNSS data for coordinates estimation as well as TRF establishment. However, the current studies only provide the estimation for satellites with PRN less than 37, hence, the PCCs should be further calibrated for the rest BDS-3 IGSO and MEO satellites. Besides, precise point positioning with multi-frequency signals show noticeable improvement in convergence time, precise modeling the measurements also require accurate multi-frequency PCC for satellites antenna, and the initial work has been done by Qu (2021) to calibrate the PCC for multi-frequency signals of BDS.

Biases of L-band data

For BDS, the well-known bias is the elevation-dependent group delay variations. It was diagnosed in BDS-2 satellites first by Wanninger and Beer (2015), and the elevation-dependent piece-wise linear models are proposed to reduce its impacts on BDS data analysis. Because of almost static observation geometry for GEO, the elevation-dependent group delay variations cannot be established with ground data. With FengYun-3C onboard data, the similar biases are identified for IGSO and MEO with the elevation angles above 40°, while larger discrepancy is observed for the elevation angles below 40° possibly due to that the measurements are smoothed (Zhao et al., 2017). This kind of bias is significantly reduced for BDS-3s and BDS-3 satellites (Zhang et al., 2017), but still show a variation of 0.1 m revealed by the measurements from a 40-m dish antenna (Zhou et al., 2018).

Another bias is the inter-system bias between BDS-2 and BDS-3 signals. By analyzing the measurements of a baseline with non-identical receiver pairs (Trimble Alloy and Septentrio POLARX5), the noticeable inter-system biases up to meter level are identified for B1I and B2b/B2I between BDS-2 and BDS-3 (Mi et al., 2021). This type of bias will cause integer wide-lane cycle difference in the MW linear combination if it is not considered. One wide-lane cycle difference has an impact of about 5 cm on the fractional part of the narrow-lane ambiguity. Therefore, narrow-lane ambiguities can be easily fixed to wrong integers, which will impact the derived orbits and clocks. Figure 6 shows the inter-system biases for the B1I and B3I ionosphere-free combination between BDS-2 and BDS-3 constellation for some stations with different types of receivers. It is clear that receiver dependent biases can be identified, and it should be noted that these values are relative instead of the absolute. For Javad receivers, the bias can be up to 5 m, while up to 3 m for Leica and Trimble receivers. Among them, the Septentrio receivers have the smallest one. Hence, we should treat BDS-2 and BDS-3 as two constellations in data processing, and ambiguity resolution as well as clock estimation must be carefully considered.

Systematic errors in ISL data

For the one-way ISL measurement, the observation corrections mainly include the orbit errors, clock offsets, the eccentrics of ISL antenna, and the hardware delays of the receiving and sending satellites. Besides, there are relativistic effect, ionosphere delay, gravitational time delay, as well as the troposphere delay in the case of the connection with an anchor station. Usually, the clock- and orbit-free observables are formed by the dual one-way measurements for orbit and clock determination (Tang et al., 2018).

The orbit-free observables mainly contain the clock offsets as well as hardware delays of the two satellites. Usually, the satellite' hardware delays are assumed constant, and the atomic clock varies linearly, especially in a short period. Hence, the residuals of orbit-free observables with the bias and linear trend removed are used as an indicator of ISL measurement noises. By linearly fitting
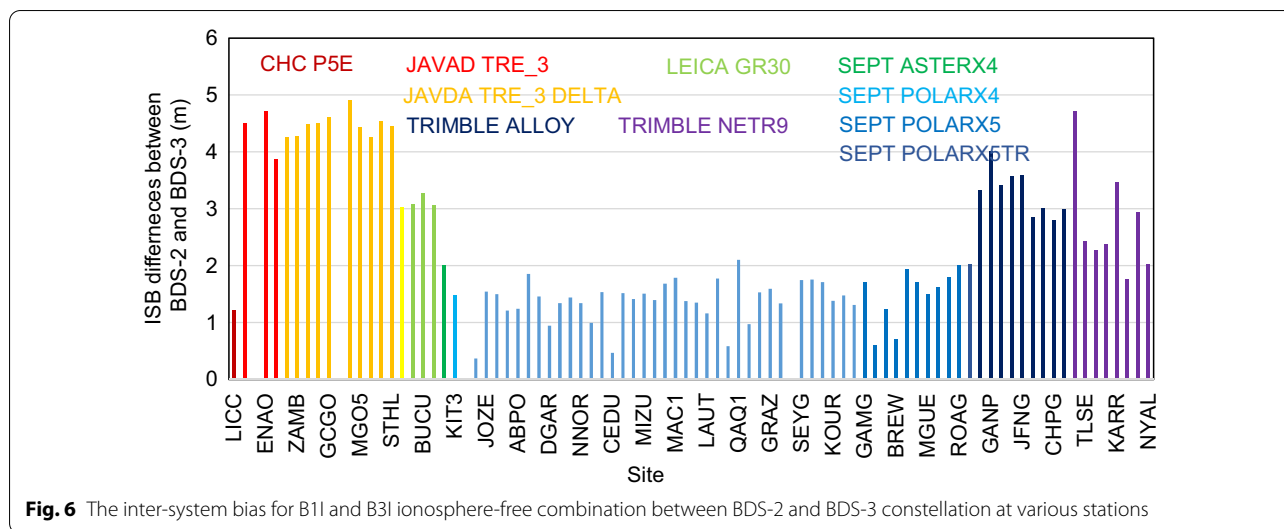
Fig. 6 The inter-system bias for B1I and B3I ionosphere-free combination between BDS-2 and BDS-3 constellation at various stations
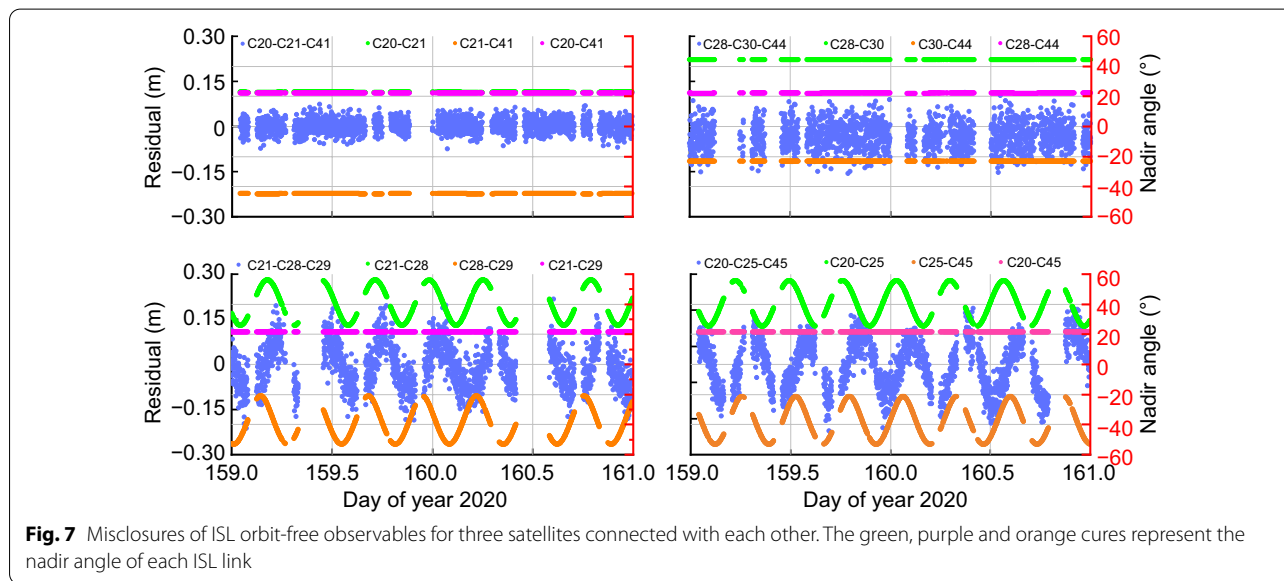

Fig. 7 Misclosures of ISL orbit-free observables for three satellites connected with each other. The green, purple and orange cures represent the nadir angle of each ISL link

the 1-h orbit-free observables, the results show that the ISL measurement noises are mainly dependent on the types of ISL terminals (Xie et al. 2019). The ISL noise for CAST satellites is about 1 cm, and around 3 cm for SECM satellites (Yang et al., 2019). However, once the orbit-free observables are detrended in long period, e.g., 24 h, the different characteristics of the in-plane links and out-of-plane links can be observed due to the appearance of other slow-varying errors (Yang et al., 2019).

As the ISLs measured in different epochs are reduced to the observables at same epoch, the closed-loop observables can be formed by more than three satellites connected with each other. For example, by summing up the three orbit-free observables, the clock offset

and hardware delays can be canceled, leaving observation noises only (Liu et al., 2020). Figure 7 shows the misclosures for four selected groups. For group of C20, C21, and C41, there are only noises, and no biases and other periodic signals are observed. However, other three groups show noticeable biases and periodic variations. The sources of these errors are still unclear, and they may be caused by the time-dependent ISL hardware delays.

Furthermore, Xie et al. (2020) identifies that the post-fit residuals of ISL clock-free observables for some satellite pairs have constant biases, as shown in Fig. 8, when the satellite-dependent transmitter and receiver hardware delays are estimated. Their analysis confirms the biases are link dependent. Hence, the biases are calibrated

Fig. 8 The post-fit residuals of ISL clock-free observables for C26-C27, C26-C32, C21-C36, and C26-C36 pairs
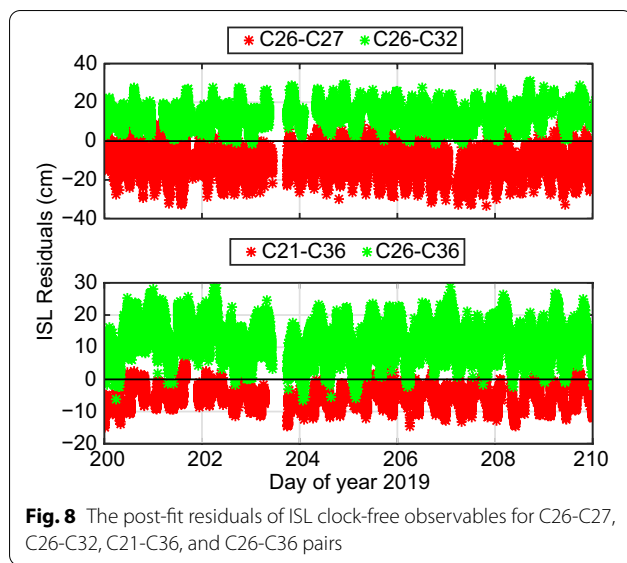
for ISL links. With these biases corrected, the post-fit residuals are noticeably reduced, and the orbit quality is improved further. However, the reason is still unknown, possibly due to the ISL antenna, whose link or channel dependent biases exist. It is also worth to note that these biases can be compensated if the link dependent biases are estimated.

Hence, the characteristics of ISL measurements require further investigation to find the sources of errors and the strategy to reduce them. Without doubt, the orbit and clock accuracy will be improved further, particularly for the clock estimated with orbit-free observables as its estimation completely depends on the accuracy of the observations. The reduction or elimination of the systematic errors in ISL observables with better observation models can further refine the stochastic model for orbit and clock determination with ISL only or combined with other measurements, e.g., L-band and SLR data.

Dynamic models
Solar radiation pressure (SRP)
As the largest non-gravitational perturbation acting on the GNSS satellite, SRP must be accurately modelled to determine the quality GNSS orbits. Various methods for SRP modeling have been proposed since 1990s, and they can be classified into three types: (1) Empirical models, e.g., the empirical CODE orbit model and its reduced or extend version (Beutler et al., 1994; Springer et al., 1999; Arnold et al., 2015). These models best fit the real GNSS tracking data, though they do not consider the actual physical forces acting on the satellite. (2) Analytical models based on the optical and geometrical properties of the satellite, e.g., Rock models (Fliegel et al., 1992;

Fliegel and Gallini 1996) and University College London model (Ziebart & Dare, 2001). The main disadvantage of these models is that they cannot compensate accurately for the real on-orbit behavior of the satellites, e.g., due to the change or uncertainty in the a priori properties of the satellite surface or deviations from nominal attitude (Rodríguez-Solano et al., 2012a). (3) Semi-analytical and semi-empirical models, e.g., the adjustable box-wing model (ABW; Rodríguez-Solano et al., 2012a) and GPS solar pressure model (GSPM; Bar-Sever & Kuang, 2004, 2005). Such models represent intermediate approaches between analytical SRP models and empirical ones and combine a good fit to real tracking data with a clear physical understanding of SRP. Among these SRP models, the reduced version of ECOM (Springer et al., 1999; labeled as ECOM1 in this study) is widely used in the GNSS community. However, it has deficiencies for SRP modeling in ON mode as well as for non-cubic satellites. Hence, the extended ECOM model (ECOM2) are proposed, or it has been augmented with a prior model.

For modeling the SRP for BDS satellites, many efforts have been made. For GEO, POD is particularly challenging due to the almost static geometry as well as the ON attitude mode employed. As a result, the strong correlations among orbital elements, SRP parameters, and ambiguities are present. To cope with these correlations, Steigenberger et al. (2013) proposed the estimation of only the D_0 of ECOM1. However, Liu et al. (2016) demonstrates that the GEO orbit can be improved by estimating six parameters (D_0, Y_0, B_0, D_s, B_s, and Y_c) instead of the typical five parameters (D_0, Y_0, B_0, B_c, and B_s) of ECOM1 model. Tan et al. (2016) developed an analytical model of SRP based on a ray-tracing approach to use as the a priori model for the ECOM1. Wang et al. (2019a) identified that the perturbation caused by the C-band communication antenna can generate the Sun-elongation-angle-dependent variation and the bias of about 14.9 cm in BDS-2 G01 SLR residuals. Besides, the ON attitude mode used by BDS GEO satellites as well as an orbital inclination of nearly 0° result in strong linear correlations between the satellite's initial position in the Z-axis and the Y_0 parameter. An empirical SRP model is established for BDS-2 GEO satellites to enhance the ECOM1 using an empirical fitting approach. Better than 10 cm Root-Mean-Square (RMS) of SLR residuals is achieved, and an improvement by 4–5 times over the ECOM1 model is obtained. However, the reduced performance is observed for WU's MGEX C01 solution after the replacement of G03 by G08, hence, the a priori model should be re-estimated.

For BDS-2 IGSO and MEO satellites, the challenge is to determine the accurate orbits in ON mode. Dramatic degeneration of orbit accuracy is first observed for BDS-2 IGSO and MEO in ON mode (Wang et al., 2013), and the
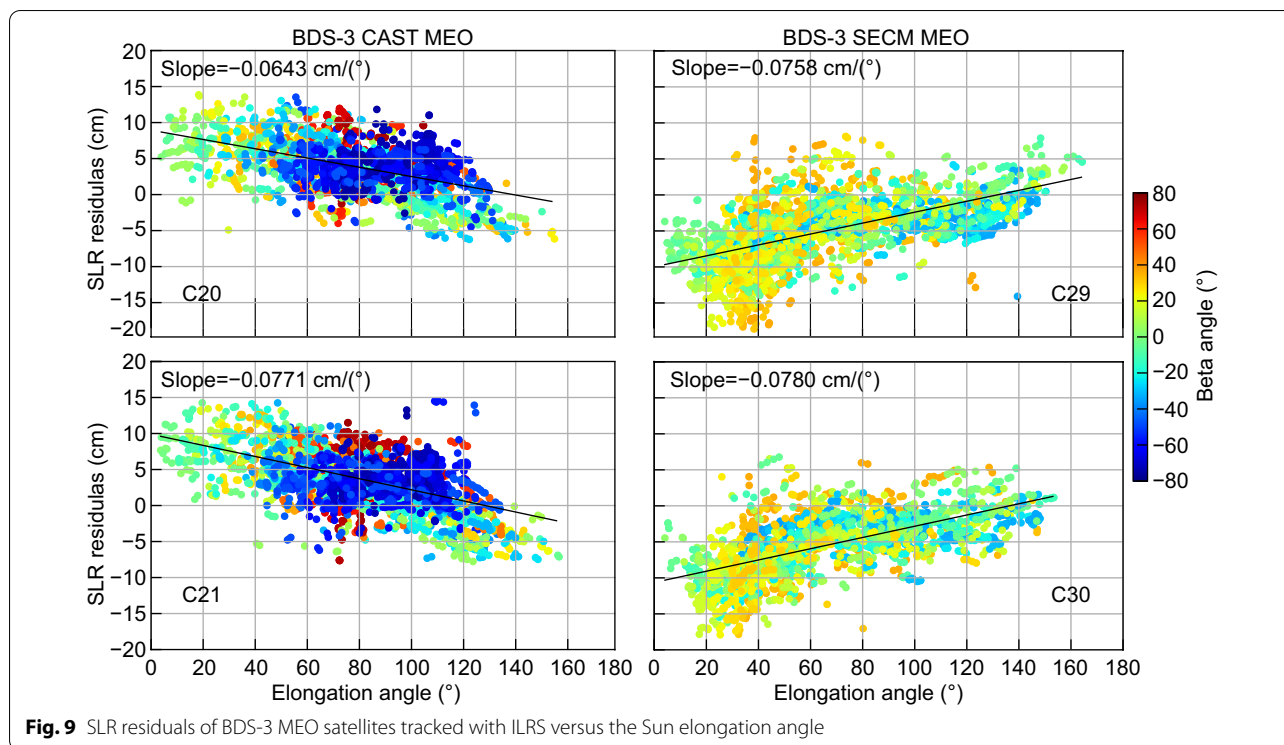
Fig. 9 SLR residuals of BDS-3 MEO satellites tracked with ILRS versus the Sun elongation angle

clear deficiencies of ECOM1 during ON mode are identified by Guo et al. (2013), Prange et al. (2016) also confirm that ECOM model are strictly designed for the satellites in YS mode. This attitude-related POD issue was analyzed by Guo et al. (2014), and the shortcomings of the ECOM1 can be compensated by adding constrained empirical accelerations in the along-track direction, resulting in significant improvement of the orbit accuracy (Zhao et al., 2013; Guo et al., 2016a). Prange et al. (2020a) also developed a series of ECOM-like empirical SRP models for the satellites in ON mode, which are slightly different for BDS-2 IGSO and MEO. The SLR validation confirms that the orbit accuracy of BDS-2 IGSO and MEO satellites can be improved by a factor of 2 in ON mode with all above models, but still lower than those in YS mode. Furthermore, semi-analytical SRP modeling for QZS-1 satellite in ON attitude is developed by Montenbruck et al. (2017b) based on a generic box-wing model, and it can also be used for modeling SRP of BDS-2 IGSO and MEO satellites in ON mode. However, few studies were conducted to demonstrate its performance for BDS satellite, and further validation is needed. To ensure a proper use of the a priori box-wing model, the optical parameters of BDS-2 satellites are estimated (Duan et al., 2019), and improvement by more than 60% over the initial values was obtained.

The ECOM1 has also been used with the emergence of BDS-3 MEO satellites. However, the SLR validations show

obvious linear systematic errors with respect to the Sun-elongation (ε) angle for MEO satellites (shown in Fig. 9), and its patterns are similar to that of Galileo IOV and FOC satellites (Montenbruck et al., 2015a; Sośnica et al., 2020). CAST and SECM MEO satellites have opposite patterns of SLR residuals with the similar absolute value of slope due to that the *Z*-bus area with transmitter antennas is much larger than the *X*-bus surface area for SECM satellites and opposite for CAST. The systematic patterns of the SLR residuals can be reduced by using the a priori box-wing or cuboid box model based on CSNO released or calibrated metadata of BDS-3 satellites (Li et al., 2020a; Duan et al., 2021a; Yan et al., 2019b), as well as the purely empirical ECOM2 model (Yan et al. 2019b). In general, better performance can be obtained for those models with calibrated optical coefficients. Besides, analyzing the estimated B_0 parameters of ECOM1 model, Li et al. (2021a) identifies that C45 (M23) and C46 (M24) satellites show different variations compared with other CAST satellites, possible due to different structure. Besides, two SECM satellites (C34/M15 and C35/M16) have relative larger D_0 with respect to other SECM satellites possible due to higher thermal radiation of solar panels or much smaller mass than the published value, as shown in Fig. 10. These mismodeling issues need further investigation.

For BDS-3 GEO and IGSO satellites, it is a challenge to model the SRP perturbations, as the additional antenna and elongated shape should be considered. Lack of
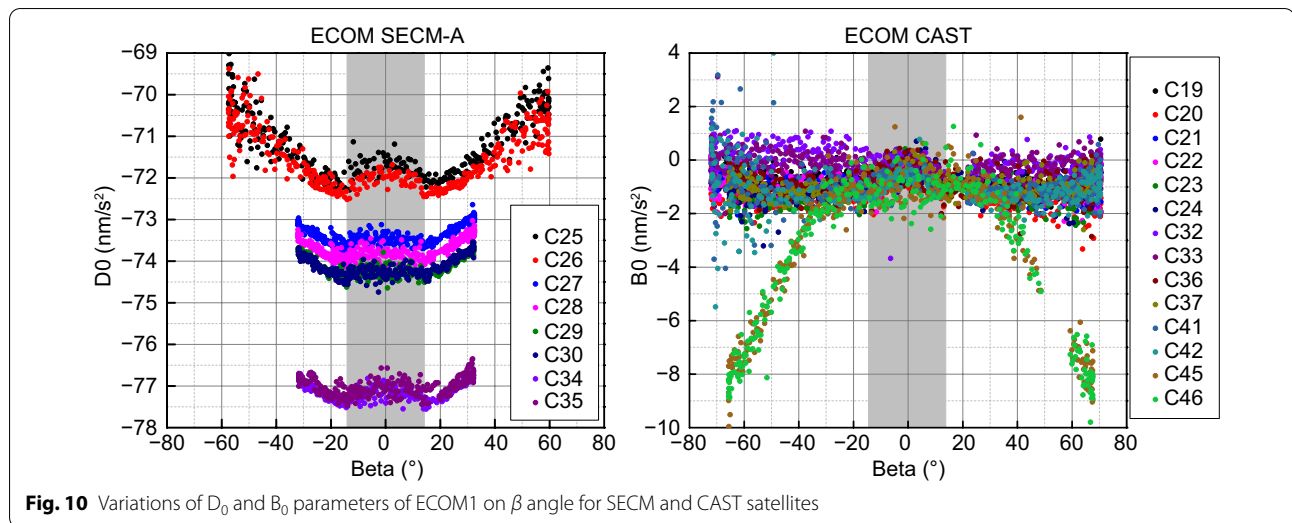
Fig. 10 Variations of D_0 and B_0 parameters of ECOM1 on β angle for SECM and CAST satellites

accurate SRP model for GEO and IGSO limits the determined orbit accuracy to the decimeter and meter level, respectively, and needs further investigation. However, the approach for the establishment of empirical SRP for BDS-2 GEO can be referenced (Wang et al., 2019a).

Antenna thrust

Antenna thrust is a perturbation along the radial direction generated by the signal transmission of satellites. The total transmitting power and the in-orbit mass of the satellite are the prerequisites for modeling this perturbation. For BDS, the mass has been disclosed by CSNO, however, the lack of total transmitting power limits the accurate modeling of antenna thrust.

Fortunately, the values are measured with a 30-m high-gain dash antenna of the German Aerospace Center (DLR) with considering the power loses along the propagation path between satellite and ground receiver by Steigenberger et al. (2018) and Steigenberger and Thoelert (2020) for BDS-2 and BDS-3 satellites, respectively. Generally, 180 W and 130 W are recommended for BDS-2 IGSO and MEO, while 310 W and 280 W are assumed for BDS-3 CAST and SECM MEO satellites. With the modelled antenna thrust, a bias in the orbit radial direction can be observed by SLR. In general, a radial effect is about 28, 5, 16, and 19 mm for BDS-2 IGSO, MEO, BDS-3 SECM MEO, and CAST MEO satellites, respectively (Guo et al., 2021). As expected, a larger bias is observed for BDS-2 IGSO than that of MEO, as the former has greater signal transmission power with the similar mass as that of MEO (see Table 1). While the orbits of BDS-3 CAST MEO satellites shift much more than that of SECM ones due to greater transmit power and lighter mass compared with SECM MEO satellites.

Earth radiation pressure

ERP is a non-gravitational perturbation caused by the reflected or re-emitted solar radiation by the Earth, which is mainly along the radial direction. Similar to the antenna thrust, the ERP mainly affects the radial component of the orbit. The detailed metadata of the satellite, including satellite dimensions, optical and infrared coefficient, are useful for modeling ERP. Rodriguez-Solano (2009) presented the model for ERP computation, and it has been applied by IGS ACs for GPS and GLONASS. With the values listed in Table 3, the impacts of ERP on BDS orbits are evaluated. SLR validation demonstrates that the radial components of orbits are biased by about 25, 20, 15, and 12 mm for BDS-2 IGSO, MEO, BDS-3 CAST MEO, and SECM MEO satellites, respectively (Guo et al., 2021).

Thermal radiation pressure

The thermal radiation of a satellite is the electromagnetic radiation emitted from the surface-covered materials of the satellite as well as its entrails and generates a perturbation, called thermal radiation pressure, to the satellite. In this study, the thermal force caused by the re-radiation of the absorbed energy from the Sun in the form of heat is indicated as Thermal Radiation Pressure (TRP), whereas the force due to the emitted heat from the thermal radiator is called Thermal Radiation (TR). Since TRP and SRP show similar characteristics as both are originated from the Sun, the former is often incorporated with SRP in a combined form. However, if the satellite is inside eclipse seasons, thermal radiation should be carefully modeled. It is believed that mismodeling its impacts limits the POD accuracy in eclipse seasons. On the other hand, the heat generated by the satellite internal subsystems is usually
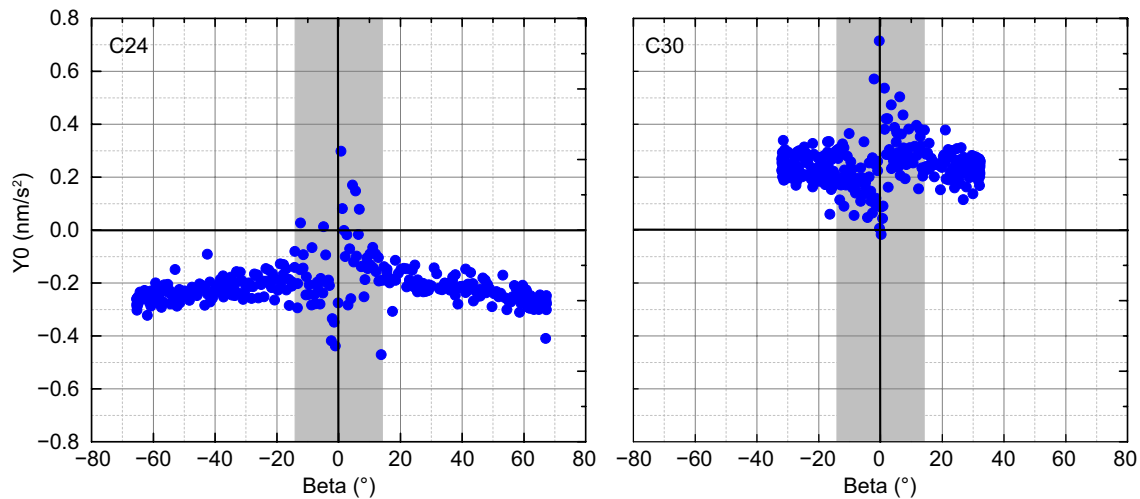
Fig. 11 Variations of Y_0 estimates for BDS-3 C24 (left) and C30 (right) satellites on β angle. Noticeable Y_0 bias is also identified for other BDS-3 satellites

vented to space via radiators or louvers on the surface of the bus. Hence, the details of the thermal radiators for a satellite are required for TR modeling. However, this kind of information is not disclosed by the spacecraft manufacturer. Usually, the radiators are assumed to be monumented on the unilluminated surfaces, i.e., $+Y$, $-Y$, and $-X$.

Recently, Sidorov et al. (2020) identified that TR force due to the emitted heat from the thermal radiator caused by the onboard atomic clock generated the orbit errors in eclipse seasons for Galileo satellites. Moreover, based on the analysis of Y_0 of ECOM1 model, the potential radiators on the $-X$ surface were identified for GLONASS satellites (Duan et al., 2020). Wang et al. (2019c) also introduced a periodic acceleration along $+X$ direction to compensate TRP for BDS satellites, particularly for C13. The systematic errors dependent of Sun elongation angle can be significantly reduced, and SLR validation indicates that the orbit accuracy is improved by 10–30% to approximately 4.5 cm and 3.0 cm for BDS-2 IGSO and MEO satellites, respectively (Wang et al., 2019a, b). Besides, some BDS-3 MEO satellites have clear radiator emissions, as their Y_0 estimates are not zero, as shown in Fig. 11. Comprehensive analysis and modeling of the radiator emission and the thermal radiation of solar panels are presented by Duan et al. (2021b) for all BDS-2 and BDS-3 satellites, and the orbit misclosures of BDS-3 satellites are reduced by a factor of two for the ECOM1 model during eclipse seasons.

Precise orbit and clock determination

In the above two sections, the observation and dynamical models for BDS POD were discussed. This section will focus on the POD strategy, and present the achievable accuracy of determined BDS orbits.

With ground and onboard L-band data.

For BDS, the ground L-band measurements are usually used for orbit determination. At the beginning, due to the limitation of tracking data a three-day solution is usually employed for orbit determination to improve the solution strength. Furthermore, the two-step approach is applied, which uses the GPS data to derive the common parameters, i.e., the station coordinates, epoch-wise receiver clock offsets, and Zenith Troposphere Delay (ZTD) parameter. They are fixed later for BDS POD. This approach benefits from the application of GPS constellation and results in a better quality for the common parameters. With this strategy, the initial POD results for BDS-2 satellites are reported by Shi et al. (2012) and Zhao et al. (2013) as well as Steigenberger et al. (2013) based on 15 BETS stations and 6 CONGO stations, respectively. Furthermore, the BDS-3s orbits are determined (Tan et al., 2017; Zhao et al., 2018). On the other hand, all parameters are estimated simultaneously from BDS only or its combination with GPS measurements, as done by Ge et al. (2012) for BDS-2 and Li et al. (2019) for BDS-3s. With the increase in tracking stations as well as their better distribution, the one-step is widely used for BDS data analysis, as used by most of IGS MGEX AC (Loyer et al., 2018; Selmke et al., 2018; Prange et al., 2020a, b), and better orbit consistency can be obtained. Currently, the BDS-2 GEO orbit consistency between

GFZ (Deutsches GeoForschungsZentrum Potsdam) and WU is at the 2–4 m level, and the best agreement of about 15 cm is achieved between GFZ and WU among all MGEX AC for IGSO and MEO satellites (Steigenberger & Mentenbruck, 2020). While the consistency in BDS-3 orbits between European Space Operations Centre of the European Space Agency (ESOC/ESA) and WU products is about 12.3, 9.2 and 4.1 cm in along-track, cross-track, and radial direction for CAST MEO satellites, while for the SECM MEO satellites there are larger mean RMS values of 25.0, 15.2 and 5.7 cm in the respective direction (Li et al., 2020b). The SLR validation demonstrates that the achieved accuracy is below 20 cm, 5–7 cm, 3.5 cm for BDS-2 GEO, IGSO, and MEO satellites, while the RMS values of 3–4 cm are achieved for BDS-3 MEO satellites using the improved SRP model (Li et al., 2020b).

To achieve the better quality of orbit solution, integer ambiguity resolution is essential. Usually, the Double-Difference (DD) ambiguities are fixed to the integers. With the development of the integer ambiguity resolution for Un-Difference (UD) ambiguities, it has been employed for GNSS POD. GFZ announced that their MGEX rapid satellite orbit and clock are estimated with the UD Ambiguity Resolution (UD-AR) using daily wide/narrow-lane Uncalibrated-Phase-Delay (UPD) method. Compared to DD, UD-AR for POD has two advantages: more phase observations can be fixed, and the selection of independent DD ambiguities can be avoided for a set of independent baselines. The 6 h orbit overlapping differences can be improved by about 30% and 18% for BDS-2 and BDS-3, respectively (Deng 2021). For BDS-3, the backup B1I and B3I signals are usually used for POD, as they are the overlapping frequencies supported by both BDS-2 and BDS-3. However, the designed signals for compatibility and interpolation are B1C and B2a, with which Li et al. (2021b) demonstrates better POD results can be obtained due to their low noises.

Besides, the LEO onboard data can also be applied for the BDS POD. The fast movement of LEO can result in a rapid change in observation geometry, and better geographical distribution of observations. Hence, it can be expected that the orbit accuracy can be improved, and the number of ground stations for achieving the required accuracy can be reduced. Zhao et al. (2017) showed that the orbit solution was enhanced by FengYun-3C onboard data. Li et al. (2020c) also presented the integrated POD for GPS, BDS, and FengYun-3C. The most pronounced benefit is observed in BDS GEO orbits, which is improved by 44% for the regional solution and 41% for the global solution. With more LEO onboard data used, the better accuracy is expected.

As the orbit and clock are determined simultaneously using the L-band data, these two types of the estimated parameters are highly correlated. To separate them, the DD approach is used for orbit determination, as CODE does in the IGS MGEX ACs. Besides, L-band Two-Way Satellite Time and Frequency Transfer (TWSTFT) and ISL are applied for time synchronization between BDS satellites and the ground master. Hence, the clocks derived from TSSTFT and ISL can be fixed for BDS POD. This approach has been used to generate the ephemeris of BDS-2 (Zhou et al., 2011; Guo et al., 2015) and BDS-3 (Pan et al., 2018; Pan et al., 2021) which are detailed by Zhou et al. (2020). Moreover, the satellite clock parameters within a relative short period can be constrained to a linear model, as GNSS onboard frequency standards are quite stable, particularly for the improved RAFSs and PHMs carried by BDS. This idea was assessed by using Galileo and BDS-2 data (Hackel et al., 2015; Qing et al., 2017). The reduction of orbit boundary discontinuities and SLR residuals is clearly observed.

Besides L-band data, the SLR measurements can also be used for the BDS POD, especially for the case of few L-band data available. For example, Hauschild et al. (2012) determined the orbit of BDS-2 M01 using the SLR tracking data. For BDS-2 IGSO and MEO, Bury et al. (2018) analyzed the impacts of orbit arc length and the number of SLR measurements on the orbits. The consistency of MEO orbits derived with SLR-only is 22.9, 13.4, and 4.4 cm in along-tack, cross-track, and radial direction, respectively, while that of BDS-2 IGSO is much worse due to the poor SLR observation geometry. As no clock to be estimated, it is expected that SLR can contribute to the improvement of the GEO orbits with a combination with L-band data (Sun et al., 2016). The bias in the microwave orbit solutions can be reduced by 20 cm using SLR measurements. However, generally, SLR's contribution to the BDS POD is marginal due to the poor distribution as well as fewer measurements.

With inter-satellite-link data.
For BDS-3 s and BDS-3 satellites, ISL technology is used to implement autonomous and global navigation with less or no ground segment supports. In this case, the orbit and clock can be precisely determined even when the satellite moves out of the coverage of ground monitoring stations. Tang et al. (2018) and Yang et al. (2017b) reported the initial POD results for BDS-3 s satellites with ISL observables only. With the deployment of BDS-3 satellites, the POD results with ISL data were presented by many researches, e.g., Wang et al. (2019b), Xie et al. (2019), and Yang et al. (2019). For the ISL-only solution, the 3D orbit consistency is less than 20 and 30 cm for MEO and GEO/IGSO, respectively. Once the ISL data is combined with the ground tracking data, the 3D accuracy is improved to 7 cm, 13 and 20 cm for MEO, IGSO,

and GEO, respectively (Lv et al., 2020). For the ISL-only clock estimation, although the accuracy of the clock estimated by ISL observations is about 0.2–0.3 ns due to larger noises of ISL, the estimated clocks are free of orbit errors (Xie et al., 2020) and show better stability in a long period. The analysis performed by Cai et al. (2020) indicated that the ISL data from different orbit planes contribute to POD more than that from the same plane, as they have better observation geometry.

Instead of processing the clock-free and orbit-free ISL measurements for orbit and clock determination, Ruan et al. (2020) proposed a method to process the raw ISL measurements directly to obtain satellite orbits, clocks, and hardware delays of ISL equipment simultaneously. Compared with the dual-way model, it can process ISL observables as much as possible, and obtain consistent orbit and clock solutions. However, the clock will be potentially contaminated by the orbit errors.

Orbit and clock products

Currently, iGMAS and IGS MGEX provide the BDS orbits. Five ACs contribute BDS-2 and BDS-3 products to IGS MGEX routinely, i.e., CODE, GFZ, Shanghai Astronomical Observatory (SHAO), Information and Analysis Center (IAC), and WU, while 13 ACs to iGMAS. Although WU and SHAO are the ACs for both MGEX and iGMAS, different solutions are submitted to each project. Among MGEX ACs, CODE does not provide BDS GEO solutions. Besides, ESOC/ESA has also been providing BDS-3 orbit and clock solutions since DOY 1, 2019 (http://navigation-office.esa.int/products/gnss-products/). Within iGMAS, the ultra-rapid, rapid, and final products for BDS are generated from those submitted by all ACs, while only WU releases its hourly ultra-rapid Multi-GNSS solutions to support (near) real-time applications. The consistency in the orbit and clock products for each AC with respect to the combined solutions is presented on the iGMAS website (http://www.igmas.org). For IGS MGEX, the consistency in the MGEX orbit products is assessed by comparing the results from different ACs, whereas their accuracy is evaluated by SLR residuals. Complementary plots of such quality assessments are presented on the MGEX website with weekly updates (see https://igs.org/mgex/analysis), and summarized by Steigenberger and Montenbruck (2020). Guo et al. (2016b) made a comprehensive assessment of the MGEX BDS orbit products from January 1, 2013, to May 1, 2015. As the successor, Li et al. (2020b) have assessed the products quality since 2018.
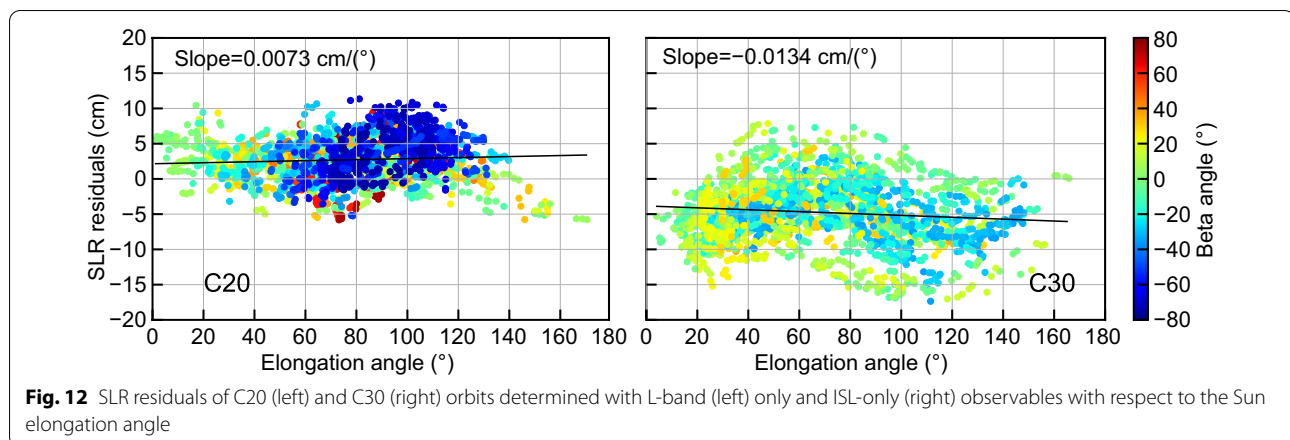
As the orbit and clock solutions have been provided by many ACs, it is possible to implement the Multi-GNSS combination. This has been done within iGMAS (Chen et al., 2015). IGS Analysis Center Coordinator initiated an experimental Multi-GNSS orbit combination service in 2019 by adapting the combination software used for many years for IGS GPS and GLONASS combinations. The Multi-GNSS orbits are combined based on the individual products generated by IGS and MGEX ACs. The validation performed by Sośnica et al. (2020) demonstrated the good quality achieved for the combined solutions. However, the BDS-3 MEO satellites suffer the orbit errors for mismodeling SRP. This is expected, as ECOM1 model is used to generate the WU BDS-3 orbits in the selected period. The mean standard deviations of SLR residuals are 87, 51, 40 mm for BDS-2 GEO, IGSO, and MEO satellites, respectively. Besides, WU also release the combined orbits for Multi-GNSS satellites based on the MGEX AC products (Chen et al., 2020).

Consistent orbits and clocks from ISL and L band data

Previous studies demonstrated that the SLR residuals of BDS-3 CAST and SECM MEO satellite orbits determined with the ground L-band data had linear trend but opposite dependency with respect to the position of Sun. Usually, this behavior is believed to be caused by the large area-to-mass ratio as well as the elongated shape. With the ISL data only in 2019, the orbits for those satellites are determined based on ECOM1 model. However, the linear variations in the SLR residuals with respect to Sun-elongation angle are significantly reduced, as shown in Fig. 12 for C20 and C30. The possible explanation is that the observations have different sensitivity to the satellite position in each direction. The ground L-band data can only capture the variations in radial direction, while ISL data observe the orbit errors in along-track more precisely, resulting in the precise estimation of SRP along D direction. This explanation needs further investigation.

Besides, the different characteristics are also observed for the clocks determined with L-band and ISL data separately, as shown in Xie et al. (2020). As the noise level of Ka-band ISL measurements is about 10 times higher than that of the L-band carrier phase observations, the clocks derived with ISL data display a superposition of random walk and white noises, and the corresponding Allan Derivation (ADEV) with the sampling interval of 2000 s is generally worse than that of the L-band clocks. However, a pronounced "bump" appears at around second 20,000 for ADEV of the L-band clocks, as the clocks are contaminated by the orbit errors, while ISL derived clock do not show such behaviors. The spectra analysis also demonstrates that ISL and L-band clocks have different characteristics. For L-band clocks, there are pronounced 1-CPR (cycle-per-revolution), 2-CPR, and 3-CPR harmonics. However, only 1-CPR and 2-CPR signals are observed for ISL clocks. And the amplitude of 1-CPR is only a half of that of L-band clocks. These indicate the orbit errors are

Fig. 12 SLR residuals of C20 (left) and C30 (right) orbits determined with L-band (left) only and ISL-only (right) observables with respect to the Sun elongation angle

significantly reduced within ISL clocks. Hence, for the clock estimation with the L-band and ISL data, it is not just a simple combination of the measurements, but the different characteristics of both types of data needs considering to get clock products with good stability in both short and long periods.

Contributions to geodetic parameters estimation

In addition to the PNT services, GNSS also play a fundamental role in the establishment of the TRF with the estimation of the EOP, geocenter, and terrestrial station coordinates with orbit and clock simultaneously. These geodetic parameters are time-variable with a geophysical origin. Theoretically, their estimates should be independent of the GNSS constellation. However, the spurious draconitic signals are identified in the GNSS-based estimates originated from orbit modeling issues (especially the SRP) and GNSS constellation characteristics. As shown by Scaramuzza et al. (2018), 3 instead of 6 orbital planes in the constellation may lead to spurious signals in polar motion, especially at the harmonic of 3 cycles per draconitic year (cpy). Hence, the spurious signals in polar motion can be expected for BDS as 3 orbital planes used. And serious collinearity issues due to the simultaneous estimation of epoch-wise station positions and satellite clock offsets and tropospheric parameters in global GNSS data analyses contaminate the determination of all three components of geocenter (Rebischung et al., 2014). To improve the estimation, the collinearity issues can be reduced by the simultaneous analysis of Multi-GNSS data collected by ground stations and LEO satellites, the modelling of ultra-stable satellite docks, and the mitigation of orbit modelling errors (Rebischung et al., 2014). Zajdel et al. (2020, 2021) investigated the contribution of Multi-GNSS to the estimation of EOP and geocenter with the focus on the SRP modeling and length of orbit arc. However, the contribution of BDS, particularly BDS-3, is

less investigated. Xu et al. (2014) investigated the impacts of BDS-2 on the EOP estimation with a combination of GPS. Recently, Duan et al. (2021) analyzed the impacts of BDS SRP models on EOP and geocenter estimation and show that the use of the a priori box-wing model can mitigate a large portion of the spurious signals in the geodetic parameters.

Another issue for the GNSS contribution to TRF is its weak ability to determine the terrestrial scale, as it cannot be separated from conventional satellite PCOs. Two approaches can be used to overcome the issue. One is to fix the transmitter antenna patterns of at least one satellite, and the other is to use LEO onboard data for the PCO estimation because the orbits of the LEOs are scale independent. Although the PCO values are not available for GPS and GLONASS satellites, the ground calibrated PCO values for Galileo, BDS, and QZSS have been released, making a reliable estimation of the terrestrial scale with GNSS possible. The preliminary estimation by Qu et al. (2021) demonstrates that the scale inconsistency derived from BDS and Galileo released PCOs reaches about $+1.854 \pm 0.191$ ppb (part-per-billion). Hence, more efforts should be made to bridge the gap to obtain a consistent scale determined by different GNSS constellations. One of the possible ways is to use the onboard BDS, Galileo, and GPS data from LEO satellites, as done by Huang et al. (2021).

Besides ground and onboard L-band data, BDS also provide ISL measurements, which has potential for geodetic estimation. The simulation performed by Glaser et al. (2020) assess the potential improvements of the Kepler constellation on the TRF origin and scale. The results demonstrate that the fully developed Kepler system significantly improves the geocenter estimates, as it increases the reliability due to a complete de-correlation of the geocenter coordinates and the orbit parameters related to the SRP modeling. The inclusion of ISL can also

make the estimation of the Z component of geocenter better by a factor of 13. However, the preliminary validation demonstrates the BDS ISL has marginal impacts on the estimation of geodetic parameters (Guo et al., 2020). This is possibly due to larger noises (2–3 cm) of BDS Ka-band ISL than that of Kapler laser ISL (1 mm) as well as unmodelled systematic errors in BDS ISL data as shown above. Hence, the ability of BDS for geodetic parameter estimation with ISL should be explored further.

Summary and conclusion

Since the development of BDS, substantial process in the model and strategy for BDS POD have been made. The expanding tracking network and the disclosed metadata lay the vital foundation for the refinement of observation model and dynamic model for BDS POD. Initial orbit and clock solutions have been made publicly available to support precise positioning and to identify the weaknesses of POD strategy. Noticeable improvements in the calibration of the PCCs for receiver and transmitter antennas, yaw attitude, biases, SRP modeling, and antenna thrust have been made. POD with ISL measurements also achieves a great success. The SLR validation shows the accuracy of BDS-3 orbits is at similar level as GPS, however, the consistency of the orbit is still lower than that of GPS. Besides, the further study of new ISL measurements are still needed regarding its characteristics and systematic errors to explore the potential not only in orbit and clock determination, but also in geodetic parameter estimation. Hence, the following works remain to be done to improve BDS POD accuracy.

- Further disclosure of the completed and detailed spacecraft parameters, e.g., the completed dimensions, optical coefficients as well as transmitting power, by the manufactures or system provider.
- Calibration of the PCOs and PCVs for all BDS satellites based on the IGS recommended PCCs of receiver antennas using the ground and LEO onboard data.
- Further refinement of the SRP perturbation for BDS satellites, particularly for BDS-2 IGSO and MEO in ON mode as well as BDS-3 IGSO and MEO satellites with the consideration of the additional antennas and different characteristics of satellite groups.
- Modeling the thermal radiation for better orbit determination and predication in eclipse seasons.
- Investigation of the characteristics of ISL measurements for mitigating the observation errors.
- Analysis of the contribution of the L-band and ISL data to orbit and clock products, and investigation of the sources of SRP-deduced orbit errors.

- Orbit determination with short-term clock modeling for ultra-stable clock or clock-free measurements.
- Full exploration of the BDS contribution to geodetic estimation as well as the establishment of terrestrial reference frame with the focus on the scale and origin.

No doubt, these tasks should be investigated in a close cooperation with the manufacturers and system provider. Better orbit solution for BDS will be obtained with the combination of various kinds of observations.

Authors' contributions
Q.Z.: review, editing. J.Guo: original draft, review & editing the manuscript. Chen Wang: writing satellite metadata and SRP modeling. Yifei Lv: ISL data procession; Xiaolong Xu: EOP and antenna modeling. Chao Yang: Tracking data. Junqiang Li: orbit and clock products. All authors read and approved the final manuscript.

Declarations

Competing interests
The author(s) declare(s) that they have no competing interests.

Author details
[1]GNSS Research Center, Wuhan University, 129 Luoyu Road, Wuhan 430079, China. [2]School of Geological Engineering and Geomatics, 126 Yanta Road, Xi'an 710064, China. [3]School of Geodesy and Geomatics, Wuhan University, 129 Luoyu Road, Wuhan 430079, China.

References

Arnold, D., Meindl, M., Beutler, G., Dach, R., Schaer, S., Lutz, S., et al. (2015). CODE's new solar radiation pressure model for GNSS orbit determination. *Journal of Geodesy, 89,* 775–791. https://doi.org/10.1007/s00190-015-0814-4.

Bar-Sever, Y. E. (1996). A new model for GPS yaw attitude. *Journal of Geodesy, 70*(11), 714–723. https://doi.org/10.1007/BF00867149.

Bar-Sever, Y., & Kuang, D. (2004). *New empirically derived solar radiation pressure model for global positioning system satellites* (pp. 42–159). The Interplanetary Network Progress Report.

Bar-Sever, Y., & Kuang, D. (2005). *New empirically derived solar radiation pressure model for global positioning system satellites during eclipse seasons* (pp. 42–160). The Interplanetary Network Progress Report.

Beutler, G., Brockmann, E., Gurtner, W., Hugentobler, U., Mervart, L., Rothacher, M., & Verdun, A. (1994). Extended orbit modeling techniques at the CODE processing center of the international GPS service for geodynamics (IGS): Theory and initial results. *Manuscripta Geodaetica, 19*(6), 367–386.

Bury, G., Sosnica, K., & Zajdel, R. (2018). Multi-GNSS orbit determination using satellite laser ranging. *Journal of Geodesy, 93*, 2447–2469. https://doi.org/10.1007/s00190-018-1143-1.

CSNO (2019b). Definitions and descriptions of BDS/GNSS satellite parameters for high precision application. http://www.beidou.gov.cn/yw/gfgg/201912/W020200323534413026471.doc. Accessed 1 September 2021.

CSNO (2019a). Satellite Information of BDS, China Satellite Navigation Office. http://en.beidou.gov.cn/SYSTEMS/Officialdocument/201912/P020200103556125703019.rar. Accessed 1 September 2021.

Cai, H., Meng, Y., Geng, T., & Xie, X. (2020). Initial results of precise orbit determination using satellite-ground and inter-satellite link observations for BDS-3 satellites. *Geomatics and Information Science of Wuhan University, 45*, 1493–1500. https://doi.org/10.13203/j.whugis20180499.

Chen, Z., & Wu, X. (2020). General design of the third generation BeiDou navigation satellite system. *Journal of Nanjing University of Aeronautics & Astronautics, 52*, 6. https://doi.org/10.16356/j.1005-2615.2020.06.001.

Chen, Q., Yang, H., Chen, Z., Wang, H., & Wang, C. (2019). Solar radiation pressure modeling and application of BDS satellite. *Acta Geodaeticaet Cartographica Sinica, 48*(2), 169–175. https://doi.org/10.11947/j.AGCS.2019.20180097.

Chen, X., Zhao, S., Wang, M., & Lu, M. (2016). Space-borne BDS receiver for LING QIAO satellite: Design, implementation and preliminary in-orbit experiment results. *GPS Solutions, 20*, 837–847. https://doi.org/10.1007/s10291-015-0493-x.

Chen, G., Guo, J., Geng, T., & Zhao, Q. (2020). Multi-GNSS orbit combination at Wuhan University: strategy and preliminary products. *Journal of Geodesy* (under review).

Chen, K., Xu, T., Chen, G., Li, J., & Yu, S. (2015). The orbit and clock combination of iGMAS analysis centers and the analysis of their precision. In Sun et al. (Ed.), China satellite navigation conference (CSNC) 2015 proceedings: Volume II. Lecture Notes in Electrical Engineering (Vol. 341). Berlin, Heidelberg: Springer. https://doi.org/10.1007/978-3-662-46635-3_36.

Dai, X., Ge, M., Lou, Y., Shi, C., Wickert, J., & Schuh, H. (2015). Estimating the yaw-attitude of BDS IGSO and MEO satellites. *Journal of Geodesy*, 89(10), 1005–1018. https://doi.org/10.1007/s00190-015-0829-x

Deng, Z. (2021). WL_UPD, integer clock and OBX from GFZ MGEX RAPID products. IGSMAIL-8068.

Dilssner, F., Springer, T., Gienger, G., & Dow, J. (2011). The GLONASS-M satellite yaw-attitude model. *Advances in Space Research, 47*(1), 160–171. https://doi.org/10.1016/j.asr.2010.09.007.

Dilssner, F., Springer, T., Schönemann, E., & Enderle, W. (2014). Estimation of satellite antenna phase center corrections for BeiDou. In *Proceedings of IGS workshop 2014*, 23–27 June 2014, Pasadena, USA.

Dilssner, F. (2017). A note on the yaw attitude modeling of BeiDou IGSO-6. http://navigation-office.esa.int/attachments_24576369_1_BeiDou_IGSO6_Yaw_Modeling.pdf. Accessed 21 September 2021.

Dilssner, F., Springer, T., Schönemann, & Enderle, W. (2018). *Initial orbit determination of third-generation BeiDou MEO spacecraft*. IGS Workshop 2018, 28 Oct -2 Nov 2018, Wuhan, China

Duan, B., Hugentobler, U., Hofacker, M., & Selmke, I. (2020). Improving solar radiant pressure for GLONASS satellites. *Journal of Geodesy, 94*, 72. https://doi.org/10.1007/s00190-020-01400-9.

Duan, B., Hugentobler, U., & Selmke, I. (2019). The adjusted optical properties for Galileo/BeiDou-2/QZS-1 satellites and initial results on BeiDou-3e and QZS-2 satellites. *Advances in Space Research, 63*(5), 1803–1812. https://doi.org/10.1016/j.asr.2018.11.007.

Duan, B., Hugentobler, U., Selmke, I., & Marz, S. (2021a). Physical a priori solar radiation pressure models for GNSS satellites with focus on BDS. EGU2021, vPICOonline, 27.Apr, 2021, EGU21-12358.

Duan, B., Hugentobler, U., Selmke, I., Marz, S., Killian, M., & Rott, M. (2021b). *BeiDou satellite radiation force models for precise orbit determination and geodetic applications*. TechRxiv. Preprint. https://doi.org/10.36227/techrxiv.15111978.v1

Fliegel, H., & Gallini, T. (1996). Solar force modeling of block IIR global positioning system satellites. *Journal of Spacecraft and Rockets, 33*(6), 863–866. https://doi.org/10.2514/3.26851.

Fliegel, H., Gallini, T., & Swift, E. (1992). Global positioning system radiation force model for geodetic applications. *Journal of Geophysical Research*, 97(B1), 559–568. https://doi.org/10.1029/91JB02564

Ge, M., Zhang, H. P., Jia, X. L., Song, S. L., & Wickert, L. (2012). What is achievable with the current COMPASS Constellations? In *Proceedings of the 25th international technical meeting of the satellite division of the institute of navigation (ION GNSS 2012)*, Nashville, 17–21 September 2012.

Glaser, S., Michalak, G., Männel, B., König, R., Neumayer, K. H., & Schuh, H. (2020). Reference system origin and scale realization with the futhre GNSS constellation "Kapler". *Journal of Geodesy*, 94, 117. https://doi.org/10.1007/00190-020-01441-0

Guo, J. (2014). *The impacts of attitude, solar radiation and function model on precise orbit determination for GNSS satellites*. PhD Dissertation, GNSS Research Center, Wuhan University.

Guo, J., Chen, G., Zhao, Q., Liu, J., & Liu, X. (2017). Comparison of solar radiation pressure models for BDS IGSO and MEO satellites with emphasis on improving orbit quality. *GPS Solutions, 21*, 511–522. https://doi.org/10.1007/s10291-016-0540-2.

Guo, F., Li, X., Zhang, X., & Wang, J. (2016b). Assessment of precise orbit and clock products for Galileo, BeiDou, and QZSS from IGS Multi-GNSS Experiment (MGEX). *GPS Solution, 21*, 279–290. https://doi.org/10.1007/s10291-016-0523-3.

Guo, J., Xu, X., Zhao, Q., & Liu, J. (2016a). Precise orbit determination for quad-constellation satellites at Wuhan University: Strategy, result validation, and comparison. *Journal of Geodesy, 90*, 143–159. https://doi.org/10.1007/s00190-015-0862-9.

Guo, R., Zhou, J., Hu, X., Liu, L., Tang, B., Li, X., & Wu, S. (2015). Precise orbit determination and rapid orbit recovery supported by time synchronization. *Advances in Space Research, 55*(12), 2889–2898. https://doi.org/10.1016/j.asr.2015.03.001.

Guo, J., Zhao, Q., Geng, T., Su, X., & Liu, J. (2013). Precise orbit determination for COMPASS IGSO satellites during yaw maneuvers. In J. Sun, W. Jiao, H. Wu, & C. Shi (Eds.), *Proceedings China satellite navigation conference (CSNC) 2013* (Vol. III, no. 245, pp. 41–53). Springer. https://doi.org/10.1007/978-3-642-37407-4_4.

Guo, J., & Zhao, Q. (2014). *Analysis of precise orbit determination for Beidou satellites during yaw maneuvers*. Presented at China Satellite Navigation Conference (CSNC) 2014, Wuhan, 22 May 2014.

Guo, J., Qu, Z., Chao, Y., Chen, G., Wang, C., & Zhao, Q. (2020). *The potential contributions and challenges of BDS to establishment of terrestrial reference frame*. Presented at China Satellite Navigation Conference (CSNC) 2020, Chengdu, 23 November 2014.

Guo, J., Wang, C., & Zhao, Q. (2021). BDS-3 precise orbit and clock solution at Wuhan University: status and improvement. *Journal of Geodesy* (under review)

Hackel, S., Steigenberger, P., Hugentobler, U., Uhlemann, M., & Montenbruck, O. (2015). Galileo orbit determination using combined GNSS and SLR observations. *GPS Solution, 19*(1), 15–25. https://doi.org/10.1007/s10291-013-0361-5.

Hauschild, A., Montenbruck, O., Sleewaegen, J. M., Huisman, L., & Teunissen, P. (2011). Characterization of compass M-1 signals. *GPS Solutions, 16*, 117–126. https://doi.org/10.1007/s10291-011-0210-3.

Hauschild, A., Montenbruck, O., Sleewaegen, J. M., Huisman, L., & Teunissen, P. G. (2012). Characterization of compass M-1 signals. *GPS Solutions, 16*, 117–126. https://doi.org/10.1007/s10291-011-0210-3.

Huang, W., Männel, B., Brack, A., & Schuh, H. (2021). Two methods to determine scale-independent GPS PCOs and GNSS-based terrestrial scale: Comparison and cross-check. *GPS Solution, 25*, 4. https://doi.org/10.1007/s10291-020-01035-5.

Huang, G., Yan, X., Zhang, Q., Liu, C., Wang, L., & Qin, Z. (2018). Estimation of antenna phase center offset for BDS IGSO and MEO satellites. *GPS Solution, 22*, 49. https://doi.org/10.1007/s10291-018-0716-z.

Jiao, W., Ding, Q., Li, J., Lu, X., Feng, L., Ma, J., & Chen, G. (2011). Monitoring and assessment of GNSS open services. *Journal of Navigation, 64*(S1), S19–S29. https://doi.org/10.1017/s0373463311000385.

Krzan, G., Dawidowicz, K., & Wielgosz, P. (2020). Antenna phase center correction differences from robot and chamber calibrations: The

Zhao et al. Satellite Navigation   *(2022) 3:2*

Page 22 of 24

case study LEIAR25. *GPS Solutions, 24*, 747. https://doi.org/10.1007/s10291-020-0957-5.

Kröger, J., Kersten, T., Breva, Y., & Schön, S. (2021). Multi-frequency multi-GNSS receiver antenna calibration at IfE: Concept—Calibration results—Validation. *Advances in Space Research*. https://doi.org/10.1016/j.asr.2021.01.029.

Li, X., Hu, X., Guo, R., Tang, C., Zhou, S., Liu, S., & Chen, J. (2018). Orbit and positioning accuracy for new generation BeiDou satellites during the earth eclipsing period. *The Journal of Navigation, 71*, 1069–1087. https://doi.org/10.1017/S0373463318000103.

Li, J., Yuan, Y., Huang, S., Liu, C., Lou, J., & Li, X. (2021). Examination and enhancement of solar radiation pressure model for BDS-3 satellites. EGU2021, vPICOonline, 27.Apr, 2021, EGU21-12358171635.

Li, R., Wang, N., Li, Z., Shang, Y., Wang, Z., & Ma, H. (2021b). Precise orbit determination of BDS-3 satellites using B1C and B2a dual-frequency measurements. *GPS Solutions, 25*, 95. https://doi.org/10.1007/s10291-021-01126-x.

Li, X., Yuan, Y., Zhu, Y., Huang, J., Wu, J., Xiong, Y., et al. (2019). Precise orbit determination for BDS3 experimental satellites using iGMAS and MGEX tracking networks. *Journal of Geodesy, 93*, 103–117. https://doi.org/10.1007/s00190-018-1144-0.

Li, X., Yuan, Y., Zhu, Y., Jiao, W., Bian, L., Li, X., & Zhang, K. (2020a). Improving BDS-3 precise orbit determination for medium earth orbit satellites. *GPS Solution, 24*, 53. https://doi.org/10.1007/s10291-020-0967-3.

Li, X., Zhu, Y., Zheng, K., Yuan, Y., Liu, G., & Xiong, Y. (2020b). Precise orbit and clock products of galileo, BDS and QZSS from MGEX Since 2018: Comparison and PPP validation. *Remote Sensing, 2020*(12), 1415. https://doi.org/10.3390/rs12091415.

Li, X., Zhang, K., Meng, X., Zhang, Q., Zhang, W., Li, X., & Yuan, Y. (2020c). LEO-BDS-GPS integrated precise orbit modeling using FengYun-3D, FengYun-3 C onboard and ground observations. *GPS Solutions, 24*, 48. https://doi.org/10.1007/s10291-020-0962-8.

Li, X., Zhang, K., Meng, X., Zhang, W., Zhang, Q., Zhang, X., & Li, X. (2020d). Precise orbit determination for the FY-3 C satellite using onboard BDS and GPS observations from 2013, 2015, and 2017. *Engineering, 6*(8), 904–913. https://doi.org/10.1016/j.eng.2019.09.001.

Liu, C., Gao, W., Pan, J., Tang, C., Hu, X., Wang, W., et al. (2020). Inter-satellite clock offsets adjustment based on closed-loop residual detection of BDS inter-satellite link. *Acta Geodaetica et Cartographica Sinica, 49*(9), 1149–1157. https://doi.org/10.11947/j.AGCS.2020.20200319.

Liu, J., Gu, D., Ju, B., Shen, Z., Lai, Y., & Yi, D. (2016). A new empirical solar radiation pressure model for BeiDou GEO satellites. *Advances in Space Research, 57*(1), 234–244. https://doi.org/10.1016/j.asr.2015.10.043.

Lin, X., Lin, B., Liu, Y., Xiong, S., Bai, T. (2018). Satellite Geometry and Attitude Mode of BDS-3 MEO Satellites Developed by SECM. Proceedings of the 31st International Technical Meeting of the Satellite Division of The Institute of Navigation (ION GNSS+ 2018), Miami, Florida, September 2018, pp. 1268–1289.

Loyer, S., Perosanz, F., Versini, L., Katsigianni, G., Mercier, F., & Mezerette. (2018). *CNES/CLS IGS analysis center: recent activities.* IGS Workshop 2018, 29 October to 2 November, Wuhan, China.

Lv, Y., Geng, T., Zhao, Q., Xie, X., Zhang, F., & Wang, X. (2020). Evaluation of BDS-3 orbit determination strategies using ground-tracking and inter-satellite link observation. *Remote Sensing, 12*(16), 2647. https://doi.org/10.3390/rs12162647.

Mi, X., Sheng, C., El-Mowafy, A., & Zhang, B. (2021). Characteristics of receiver-related biases between BDS-3 and BDS-2 for five frequencies including inter–system biases, differential code biases, and differential phase biases. *GPS Solutions, 25*, 113. https://doi.org/10.1007/s10291-021-01151-w.

Montenbruck, O., Hauschild, A., & Hessels, U. (2011). Characterization of GPS/GIOVE sensor stations in the CONGO network. *GPS Solution, 15*(3), 193–205. https://doi.org/10.1007/s10291-010-0182-8.

Montenbruck, O., Schmid, R., Mercier, F., Steigenberger, P., Noll, C., Fatkulin, R., et al. (2015b). GNSS satellite geometry and attitude models. *Advances in Space Research, 56*(6), 1015–1029. https://doi.org/10.1016/j.asr.2015.06.019.

Montenbruck, O., Steigenberger, P., & Darugna, F. (2017b). Semi-analytical solar radiation pressure modeling for QZS-1 orbit-normal and yaw-steering attitude. *Advances in Space Research, 59*(8), 2088–2100. https://doi.org/10.1016/j.asr.2017.01.036.

Montenbruck, O., Steigenberger, P., & Hugentobler, U. (2015a). Enhanced solar radiation pressure modeling for Galileo satellites. *Journal of Geodesy, 89*(3), 283–297. https://doi.org/10.1007/s00190-014-0774-0.

Montenbruck, O., Steigenberger, P., Prange, L., Deng, Z., Zhao, Q., Perosanz, F., et al. (2017a). The Multi-GNSS experiment (MGEX) of the international GNSS service (IGS)—Achievements, prospects and challenges. *Advances in Space Research, 59*, 1671–1697. https://doi.org/10.1016/j.asr.2017.01.011.

Pan, J., Hu, X., Zhou, S., Tang, C., Guo, R., Zhu, L., et al. (2018). Time synchronization of new-generation BDS satellites using inter-satellite link measurements. *Advances in Space Research, 61*(1), 145–153. https://doi.org/10.1016/j.asr.2017.10.004.

Pan, J., Hu, X., Zhou, S., Tang, C., Wang, D., Yang, Y., & Dong, W. (2021). Full-ISL clock offset estimation and prediction algorithm for BDS3. *GPS Solutions, 25*, 140. https://doi.org/10.1007/s10291-021-01177-0.

Pearlman, M. R., Degnan, J. J., & Bosworth, J. M. (2002). The international laser ranging service. *Advances in Space Research, 30*, 135–143. https://doi.org/10.1016/S0273-1177(02)00277-6.

Prange, L., Orliac, E., Dach, R. et al. (2017). CODE's five-system orbit and clock solution—the challenges of multi-GNSS data analysis. *J Geod, 91*, 345–360. https://doi.org/10.1007/s00190-016-0968-8

Prange, L., Beutler, G., Dach, R., Arnold, D., Schaer, S., & Jäggi, A. (2020b). An empirical solar radiation pressure model for satellites moving in the orbit-normal mode. *Advances in Space Research, 65*(1), 235–250. https://doi.org/10.1016/j.asr.2019.07.031.

Prange, L., Villiger, A., Sidorov, D., Schaer, S., Beutler, G., Dach, R., & Jäggi, A. (2020a). Overview of CODE's MGEX solution with the focus on Galileo. *Advances in Space Research, 66*(12), 2786–2798. https://doi.org/10.1016/j.asr.2020.04.038.

Qing, Y., Lou, Y., Dai, X., & Liu, Y. (2017). Benefits of satellite clock modeling in BDS and Galileo orbit determination. *Advances in Space Research, 60*(12), 2550–2560. https://doi.org/10.1016/j.asr.2017.03.040.

Qu, Z., Guo, J., & Zhao, Q. (2021). Phase center corrections for BDS IGSO and MEO satellites in IGb14 and IGSR3 frame. *Remote Sensing, 13*(4), 745. https://doi.org/10.3390/rs13040745.

Qu, Z. (2021). *Phase center corrections for BDS satellites with ground and LEO onboard data*. Master Dissertation, Wuhan University.

Rebischung, P., Altamimi, Z., & Springer, T. (2014). A collinearity diagnosis of the GNSS geocenter determination. *Journal of Geodesy, 88*, 65–85. https://doi.org/10.1007/s00190-013-0669-5.

Rebischung, P. (2014). *Can GNSS contribute to improving the ITRF definition?* PhD Thesis, Ecole Doctorale Astronomie et Astrophysique d'Ile-de-France.

Rodriguez-Solano, C., Hugentobler, U., Steigenberger, P., & Lutz, S. (2012b). Impact of earth radiation pressure on GPS position estimates. *Journal of Geodesy, 86*(5), 309–317. https://doi.org/10.1007/s00190-011-0517-4.

Rodríguez-Solano, C., Hugentobler, U., & Steigenberger, P. (2012a). Adjustable box-wing model for solar radiation pressure impacting GPS satellites. *Advances in Space Research, 49*, 1113–1128. https://doi.org/10.1016/j.asr.2012.01.016.

Rodríguez-Solano, C. (2009). *Impact of albedo modeling on GPS orbits*. Master Thesis. Technische Universität München.

Ruan, R., Jia, X., Feng, L., Zhu, J., Huyan, Z., Li, J., & Wei, Z. (2020). Orbit determination and time synchronization for BDS-3 satellites with raw inter-satellite link ranging observations. *Satellite Navigation, 1*, 8. https://doi.org/10.1186/s43020-020-0008-y.

Scaramuzza, S., Dach, R., Beutler, G., Arnold, D., Sušnik, A., & Jäggi, A. (2018). Dependency of geodynamic parameters on the GNSS constellation. *Journal of Geodesy, 92*(1), 93–104 https://doi.org/10.1007/s00190-017-1047-5.

Selmke, I., Duan, B., & Hugentobler, U. (2018). *Status of the TUM MGEX orbit and clock products*. IGS Workshop 2018, 29 October to 2 November, Wuhan, China.

Shi, C., Zhao, Q., Li, M., Tang, W., Hu, Z., Lou, Y., et al. (2012). Precise orbit determination of BeiDou satellites with precise positioning. *Science China Earth Sciences, 55*, 1079–1086. https://doi.org/10.1007/s11430-012-4446-8.

Sidorov, D., Dach, R., Polle, B., Prange, L., & Jaggi, A. (2020). Adopting the empirical CODE orbit model to Galileo satellites. *Advances in Space Research, 66*(12), 15. https://doi.org/10.1016/j.asr.2020.05.028.

Sośnica, K., Zajdel, R., Bury, G., Bosy, J., Moore, M., & Masoumi, S. (2020). Quality assessment of experimental IGS multi-GNSS combined orbits. *GPS Solutions, 24*, 54. https://doi.org/10.1007/s10291-020-0965-5.

Springer, T., Beutler, G., & Rothacher, M. (1999). A new solar radiation pressure model for GPS satellites. *GPS Solution, 2*(3), 50–62. https://doi.org/10.1007/PL00012757.

Springer, T., Agrotis, L., Dilssner, F., Feltens, J., Van Kints, M., Mayer, V., et al. (2020). The ESA/ESOC IGS analysis centre technical report 2019. http://ftp.aiub.unibe.ch/users/villiger/2019_techreport.pdf. Accessed 30 August 2021.

Steigenberger, P., Hugentobler, U., Hauschild, A., & Montenbruck, O. (2013). Orbit and clock analysis of Compass GEO and IGSO satellites. *Journal of Geodesy, 87*(6), 515–525. https://doi.org/10.1007/s00190-013-0625-4.

Steigenberger, P., & Mentenbruck, O. (2020). Consistency of MGEX orbit and clock products. *Engineering*, 6(8), 898–903. DOI: https://doi.org/10.1016/j.eng.2019.12.005

Steigenberger, P., Thoelert, S., & Montenbruck, O. (2018). GNSS satellite transmit power and its impact on orbit determination. *Journal of Geodesy*, 92, 609–624. DOI: https://doi.org/10.1007/s00190-017-1082-2

Steigenberger, P., & Thoelert, S. (2020). Initial BDS-3 transmit power analysis (with BDS-2 gain pattern)

Su, M., Zhao, Q., Guo, J., Su, X., Hu, Z., & Guo, H. (2018). Phase center calibration for receiver antenna and its impact on precise orbit determination of BDS satellites. *Acta Geodaetica et Cartographica Sinica, 47*(S0), 78–85. https://doi.org/10.11947/j.AGCS.2018.20180324.

Sun, B., Su, H., Zhang, Z., Kong, Y., & Yang, X. (2016). *GNSS GEO satellites precise orbit determination based on carrier phase and SLR observations*. IGS Workshop 2016, Feb 8-12, 2016, Sydney.

Tan, B., Yuan, Y., Wen, M., Ning, Y., & Liu, X. (2017). Initial results of the precise orbit determination for the new-generation BeiDou satellites (BeiDou-3) based on the iGMAS network. *International Journal of Geo-information, 5*, 196. https://doi.org/10.3390/ijgi5110196.

Tan, B., Yuan, Y., Zhang, B., Hsu, H., & Ou, J. (2016). A new analytical solar radiation pressure model for current BeiDou satellites: IGGBSPM. *Scientific Report, 6*, 32967. https://doi.org/10.1038/srep32967.

Tang, C., Hu, X., Zhou, S., Liu, L., Pan, J., & Chen, L. (2018). Initial results of centralized autonomous orbit determination of the new-generation BDS satellites with inter-satellite link measurements. *Journal of Geodesy, 92*, 1155–1169. https://doi.org/10.1007/s00190-018-1113-7.

Villiger, A., Dach, R., Prange, L., Jaggi, A. (2021). Extension of the IGS Repro3 ANTEX file with BeiDou and QZSS satellite antenna pattern. EGU General Assembly 2021, 23. April 2021, Vienna, Austria

Wang, C., Guo, J., Zhao, Q., & Liu, J. (2018). Yaw attitude modeling for BeiDou I06 and BeiDou-3 satellites. *GPS Solutions, 22*, 117. https://doi.org/10.1007/s10291-018-0783-1.

Wang, C., Guo, J., Zhao, Q., & Liu, J. (2019a). Empirically derived model of solar radiation pressure for BeiDou GEO satellites. *Journal of Geodesy, 93*, 791. https://doi.org/10.1007/s00190-018-1199-y.

Wang, J., Liu, G., Guo, A., Xiao, G., Wang, B., Gao, M., & Wang, S. (2020a). BDS receiver antenna phase center calibration. *Acta Geodaetica et Cartographica Sinica, 49*(3):312-321. https://doi.org/10.11947/j.AGCS.2020.20190072.

Wang, L., Xu, B., Fu, F., Chen, R., Li, T., Han, Y., & Zhou, H. (2020b). Centimeter-level precise orbit determination for the Luojia-1A satellite using BeiDou observations. *Remote Sensing, 12*, 2063. https://doi.org/10.3390/rs12122063.

Wang, C., Zhao, Q., Guo, J., Liu, J., & Chen, G. (2019b). The contribution of intersatellite links to BDS-3 orbit determination: Model refinement and comparisons. *Navigation*, 66(1), 71–82. https://doi.org/10.1002/navi.295

Wang, W., Chen, G., Guo, S., Song, X., & Zhao, Q. (2013). A study on the Beidou IGSO/MEO satellite orbit determination and prediction of the different yaw control mode. In J. Sun, W. Jiao, H. Wu, & C. Shi (Eds.), *Proceedings China satellite navigation conference (CSNC) 2013* (Vol. III, pp. 31–40). Springer. https://doi.org/10.1007/978-3-642-37407-4_3.

Wanninger, L., & Beer, S. (2015). BeiDou satellite-induced code pseudorange variations: diagnosis and therapy. *GPS Solutions, 19*, 639–648. https://doi.org/10.1007/s10291-014-0423-3.

Willi, D., Lutz, S., Brockmann, E., & Rothacher, M. (2020). Absolute field calibration for multi-GNSS receiver antennas at ETH Zurich. *GPS Solutions, 24*, 375. https://doi.org/10.1007/s10291-019-0941-0.

Wübbena, G., Schmitz, M., & Warneke, A. (2019). Geo++ absolute multi frequency GNSS antenna calibration. In *Presentation at the EUREF analysis center (AC) Workshop, October 16–17, Warsaw, Poland*. http://www.geopp.com/pdf/gpp_cal125_euref19_p.pdf. Accessed 01 September 2021.

Xia, F., Ye, S., Chen, D., & Jiang, N. (2019). Observation of BDS-2 IGSO/MEOs yaw-attitude behavior during eclipse seasons. *GPS Solutions, 23*, 71. https://doi.org/10.1007/s10291-019-0857-8.

Xia, F., Ye, S., Chen, D., Wu, J., Wang, C., & Sun, W. (2020). Estimation of antenna phase center offsets for BeiDou IGSO and MEO satellites. *GPS Solution, 24*, 90. https://doi.org/10.1007/s10291-020-01002-0.

Xie, X., Geng, T., Zhao, Q., Lv, Y., Cai, H., & Liu, J. (2020). Orbit and clock analysis of BDS-3 satellites using inter-satellite link observations. *Journal of Geodesy, 94*(7), 64. https://doi.org/10.1007/s00190-020-01394-4.

Xie, X. (2019). Precise orbit and clock determination for BDS-3 satellites using inter-satellite link observations. PhD Dissertation, GNSS Research Center, Wuhan University

Xu, T., Yu, S., & Li, J. (2014). Earth rotation parameters determination using BDS and GPS data based on MGEX network. In J. Sun, W. Jiao, H. Wu, & M. Lu (Eds.), *China satellite navigation conference (CSNC) 2014 proceedings: Volume III. Lecture Notes in Electrical Engineering* (Vol. 305). Berlin, Heidelberg: Springer. https://doi.org/10.1007/978-3-642-54740-9_26.

Yan, X., Huang, G., Zhang, Q., Wang, L., Qin, Z., & Xie, S. (2019a). Estimation of the antenna phase center correction model for the BeiDou-3 MEO satellites. *Remote Sensing, 11*, 2850. https://doi.org/10.3390/rs11232850.

Yan, X., Liu, C., Huang, G., Zhang, Q., Wang, L., Qin, Z., & Xie, S. (2019b). A priori solar radiation pressure model for BeiDou-3 MEO satellites. *Remote Sensing, 11*, 1605. https://doi.org/10.3390/rs11131605.

Yang, Y., Tang, J., & Montenbruck, O. (2017a). Chinese Navigation Satellite Systems. In P. J. Teunissen, & O. Montenbruck (Eds.), *Springer handbook of global navigation satellite systems. Springer handbooks*. Cham: Springer. https://doi.org/10.1007/978-3-319-42928-1_10.

Yang, D., Yang, J., Li, G., Zhou, Y., & Tang, C. (2017b). Globalization highlight: orbit determination using BeiDou inter-satellite ranging measurements. *GPS Solutions, 21*, 1395–1404. https://doi.org/10.1007/s10291-017-0626-5.

Yang, Y., Yang, Y., Hu, X., Chen, J., Guo, R., Tang, C., et al. (2019). Inter-Satellite Link enhanced orbit determination for BeiDou-3. *The Journal of Navigation, 73*, 115–130. https://doi.org/10.1017/S0373463319000523.

Yang, C., Guo, J., & Zhao, Q. (2021). Yaw attitudes for BDS-3 IGSO and MEO satellites: Estimation, validation and modeling with inter-satellite link observations. Submitted to Journal of Geodesy.

Zajdel, R., Sosnica, K., & Bury, G. (2021). Geocenter coordinates derived from multi-GNSS: a look into the role of solar radiation pressure modeling. *GPS Solutions*, 25, 1. https://doi.org/10.1007/s10291-020-01037-3

Zajdel, R., Sosnica, K., Bury, G., Dach, R., & Prange, L. (2020). Systemspecifc systematic errors in earth rotation parameters derived from GPS, GLONASS, and Galileo. *GPS Solutions, 24*, 74. https://doi.org/10.1007/s10291-020-00989-w.

Zhang, X., Wu, M., Liu, W., Li, X., Yu, S., Lu, C., & Wichert, J. (2017). Initial assessment of the COMPASS/BeiDou-3: New generation navigation signals. *Journal of Geodesy, 91*, 1225–1240. https://doi.org/10.1007/s00190-017-1020-3.

Zhang, X., Zhou, Y., Cong, F., Ji, J., & Sun, G. (2020). Research of the dedicated platform for BeiDou-3 satellite directly into orbit. *Astronautical Systems Engineering Technology*, 4(6), 1–8

Zhao, Q., Guo, J., Li, M., Qu, L., Hu, Z., Shi, C., & Liu, J. (2013). Initial results of precise orbit and clock determination for COMPASS navigation satellite system. *Journal of Geodesy*, 87, 475–486. https://doi.org/10.1007/s00190-013-0622-7

Zhao, Q., Wang, C., Guo, J., Bin, W., & Liu, J. (2018). Precise orbit and clock determination for BeiDou-3 experimental satellites with yaw attitude analysis. *GPS Solutions*, 22, 4. https://doi.org/10.1007/s10291-017-0673-y

Zhao, Q., Wang, C., Guo, J., Yang, G., Liao, M., Ma, H., & Liu, J. (2017). Enhanced orbit determination for BeiDou satellites with FengYun-3 C onboard GNSS data. *GPS Solutions*, 21, 1179–1190. https://doi.org/10.1007/s10291-017-0604-y

Zhao, X., Zhou, S., Ci, Y., Hu, X., Cao, J., Chang, Z., et al. (2020). High-precision orbit determination for a LEO nanosatellite using BDS-3. *GPS Solutions*, 24, 102. https://doi.org/10.1007/s10291-020-01015-9

Zheng, J. (2020). *Inter-satellite link and autonomous navigation of BDS*. Presented at China Satellite Navigation Conference (CSNC) 2020, Chengdu, 23 November 2020.

Zhou, S., Hu, X., Liu, L., He, F., Tang, C., & Pang, J. (2020). Status of satellite orbit determination and time synchronization technology for global navigation satellite system. *Chinese Astronomy and Astrophysics*, 44(1), 105–118. https://doi.org/10.1016/j.chinastron.2020.04.007

Zhou, S., Hu, X., Wu, B., Liu, L., Qu, W., Guo, R., et al. (2011). Orbit determination and time synchronization for a GEO/IGSO satellite navigation constellation with regional tracking network. *Science China Physics, Mechanics and Astronomy, 54*, 1089–1097. https://doi.org/10.1007/s11433-011-4342-9.

Zhou, R., Hu, Z., Zhao, Q., Li, P., Wang, W., He, C., et al. (2018). Elevation-dependent pseudorange variation characteristics analysis for the new-generation BeiDou satellite navigation system. *GPS Solutions, 22*, 60. https://doi.org/10.1007/s10291-018-0726-x.

Ziebart, M., & Dare, P. (2001). Analytical solar radiation pressure modelling for GLONASS using a pixel array. *Journal of Geodesy*, 75, 587–599. https://doi.org/10.1007/s001900000136

Publisher's Note

Springer Nature remains neutral with regard to jurisdictional claims in published maps and institutional affiliations.